Received: 6 April 2022 | Revised: 3 December 2022 | Accepted: 6 December 2022

DOI: 10.1002/gea.21953

RESEARCH ARTICLE

Geoarchaeology An International Journal

WILEY

Structure, evolutionary context and chronological data of the Monforte de Moyuela Roman dam (Ebro Basin, NE of Spain)

José Luis Peña-Monné[1] | María Marta Sampietro-Vattuone[2] | Uribe Agudo Paula[3] | Rosario García Giménez[4] | Arsenio Muñoz[5] | David Badia Villas[6] | María Ángeles Magallón Botaya[3]

[1]Departamento de Geografía y Ordenación del Territorio, Universidad de Zaragoza, IUCA, Zaragoza, Spain

[2]Laboratorio de Geoarqueología, Universidad Nacional de Tucumán, CONICET, San Miguel de Tucumán, Argentina

[3]Departamento de Ciencias de la Antigüedad, Universidad de Zaragoza, IPH, Zaragoza, Spain

[4]Departamento de Geología y Geoquímica, Universidad Autónoma de Madrid, Cantoblanco, Madrid, Spain

[5]Departamento de Ciencias de la Tierra, Universidad de Zaragoza, IUCA, Zaragoza, Spain

[6]Departamento de Ciencias Agrarias y del Medio Natural, Escuela Politécnica Superior, Universidad de Zaragoza, Huesca, Spain

Correspondence

José Luis Peña-Monné, Departamento de Geografía y Ordenación del Territorio, Universidad de Zaragoza, IUCA, 50009 Zaragoza, Spain.
Email: jlpena@unizar.es

Scientific editing by Kevin Walsh.

Funding information

Fondo para la Investigación Científica y Tecnológica; IUCA

Abstract

The Monforte de Moyuela dam, also known as Ermita de la Virgen del Pilar dam, is a Roman reservoir built on a tributary of the Aguasvivas River (Ebro basin, Spain). A multidisciplinary study has been carried out to investigate this kind of Roman water infrastructure. It is the fifth-highest dam (16.8 m) in the Iberian Peninsula and the seventh in the Roman Empire. The initial dam was built ca. 100 B.C.–10 A.D., probably in the period of Augustus, like other nearby Roman dams. It was quickly filled due to the extreme and generalized anthropic degradation in the basin during the Roman period. During the mid-2nd century, the wall was increased in height and its final silting was dated to the early 7th century. The study of the *opus caementicium* mortars shows constructive differences between the initial and subsequent phases of the wall. These mortars provided charcoal for dating the two phases. In addition, the stratigraphic and edaphological study of the reservoir's sedimentary fill, together with the ^{14}C ages, allowed us to reconstruct the two main activity cycles and the final siltation of the dam. Subsequently, the dam broke in two phases, which created the two stepped sections located on the current valley bottom. The data obtained allowed the creation of a geomorphological map and an evolutionary model of the valley showing the main differentiated stages, from the initial construction of the dam to its final opening. Although some remains of canals downstream of the dam have been identified, the use of this dam, which remained active for several centuries, still needs to be investigated in greater detail.

KEYWORDS

Augustus epoch, Ebro Basin, Geoarchaeology, mortars, reservoir fill, Roman dam

1 | INTRODUCTION

The Mediterranean climate is characterized by rainfall scarcity and interannual variability (Lionello et al., 2006), with long periods of drought. Therefore, the regulation of fluvial flows is important for the optimal exploitation of water resources. In Roman times, water played a role in all social activities and in guaranteeing high agricultural yields, the basis of the Empire economy (Decker et al., 2017; Erdkamp, 2005). The great Roman expansion took place in the context of a warming climate (Harper & McCormick, 2018), during the so-called Roman Climate Optimum (RCO), between ca. 100–150 years B.C. and ca. 200 years A.D. (Harper, 2017; McCormick et al., 2012). This period was exceptionally warm (Ljungqvist, 2010) but better for cereal production than present-day environments (Dermody et al., 2014). There is no consensus on the humidity at that time (Dermody et al., 2011) although significant regional variability is probable (Erdkamp, 2019). Some studies point to increasing aridity in the Western Mediterranean throughout the Roman period, accompanied by intense landscape anthropization (Currás et al., 2012; Ejarque et al., 2022; Martín-Puertas et al., 2008; Peña Monné, 2018; Peña-Monné et al., 2004).

Under such environmental conditions, dams and distributary canals were built to counter natural environmental shortages, obtain good agricultural profits, and meet other social (*termae*, *fullonicae*, *nymphaea*) or economic (mills, mining) needs. However, despite their relevance, dams are poorly understood among large Roman constructions, perhaps due to their poor conservation. Their loss of capacity due to siltation, breakage due to construction problems or large floods, abandonment, and the reclamation of their building materials for other constructions resulted, in many cases, in only a few ruins being left in the archaeological record.

According to inventories made by Fernández Casado (1961), Quintela et al. (1987), Arenillas and Castillo (2003), Castillo and Arenillas (2002), Saldaña (2011), Castillo (2015), Sánchez and Martínez (2016), and Barahona (2017), it is estimated that there are almost 70 probable Roman dams in the Iberian Peninsula. Large dams are grouped into three sets: (i) dams on fluvial tributaries of the Ebro River, NE Spain; (ii) dams from Extremadura in the Guadiana River, especially around the city of Merida (*Emerita Augusta*), and (iii) dams of the Tajo basin, south of Toledo. To date, studies have focused on the largest and best-preserved dams. Some of them are Almonacid de la Cuba dam (Aguasvivas River, tributary of the Ebro River, Figure 1) (Arenillas et al., 1995; Beltrán & Viladés, 1994; I. Hereza, 1996; I. Hereza et al., 2000; J. I. Hereza et al., 1996); Muel dam (Huerva River, Ebro River basin, Figure 1) (Arenillas et al., 2006; Magallón et al., 2016; Uribe et al., 2010, 2012, 2013, 2016); Cornalbo, Proserpina, and Consuegra dams, in the Guadiana River basin (Arenillas et al., 1992, 2007; García-Diego et al., 1983a, 1983b; Álvarez Martínez, 2007; Álvarez Martínez et al., 2002; Aranda & Sánchez Carcaboso, 2000; Aranda et al., 2006; Giles Pacheco, 2011; Martín Morales et al., 2002; Rodríguez Untoria, 2011); and Alcantarilla dam, in the Tajo River basin (Aranda & Sánchez Carcaboso, 2000; Aranda et al., 1997; Arenillas & Barahona, 2009a, 2009b; Barahona Oviedo et al., 2014; Barahona, 2018a, 2018b; Celestino, 1976; Sánchez Abal, 1977). For this reason, these are the most widely cited dams in the literature on civil constructions (Baba et al., 2018; Jansen, 1983; Mays, 2008, 2010; Schnitter, 1994; Smith, 1970, 1971; among others). These studies focus on construction and styles, and most of them lack rigorous dating, casting doubt on the Roman origin of some of them (Feijoo, 2005, 2006).

We consider that, due to their nature and function, the study of dams must comprise an integrated approach that includes environmental data, contextual records, and accurate chronological frameworks. This can be achieved via geoarchaeological approaches, as proposed here for the Monforte de Moyuela dam (hereafter, Morforte dam), also known as the Ermita de la Virgen del Pilar dam, located in the Aguasvivas River basin, an Ebro River tributary. This is a little-known dam, although it was the fifth-highest (16.8 m) in the Iberian Peninsula and seventh-highest in the Roman Empire. Previous research encompassed a brief reference to I. Hereza (1996) and Arenillas (2002, 2003) and precise data about the elements of the dam building in Arenillas et al. (2005). Our objectives were as follows: (i) to determine the geological context of the basin to assess the original distribution of the lithologies involved in the dam construction; (ii) to produce a detailed geomorphological map establishing the general context of the dam, the reservoir, and the sedimentary infill; (iii) to define the structural units of the dam and undertake mortar analyses to establish different constructive stages and relative chronologies; (iv) to determine the infill size, identify morphosedimentary units, stratigraphic records, and edaphic profiles; (v) to obtain absolute chronological datings from the dam and sedimentary records; (vi) to undertake archaeological surveys and collect complementary records of canals and other remains downstream of the dam to establish the construction functions; and finally, (vii) to develop a geomorphological evolutionary model of the dam and its sedimentary infill based on all records and place it in its Holocene paleoenvironmental context.

2 | GEOGRAPHICAL AND GEOLOGICAL SETTINGS

The study area is located in the transition between the central sector of the Iberian Ranges and the south margin of the Ebro depression (NE Spain) in Teruel province (Autonomous Community of Aragón) (Figure 1). The Monforte dam was built in the middle section of the Santa María River, part of the Aguasvivas River basin, a tributary of the Ebro River on its right side. The headwaters of the fluvial course are formed by the de la Cañada and del Prado Medio streams. These streams are located in Upper Triassic (Keuper) marls, positioned between the Cretaceous limestones, marls, and sands of the Sierra de Oriche and the Triassic dolomites of Piedrahita (Muschelkalk) (Figure 2). The Santa María River starts after the confluence of both streams. It is oriented SW-NE and enters the Cambrian and Devonian slate, sandstone and dolostone formations, with scattered volcanic outcroppings of dark-coloured dacites and andesites (Ruiz Fernández de la Lopa & Carls, 1985). Left-side tributaries come from Paleozoic outcrops, while those from the right side reach the Triassic

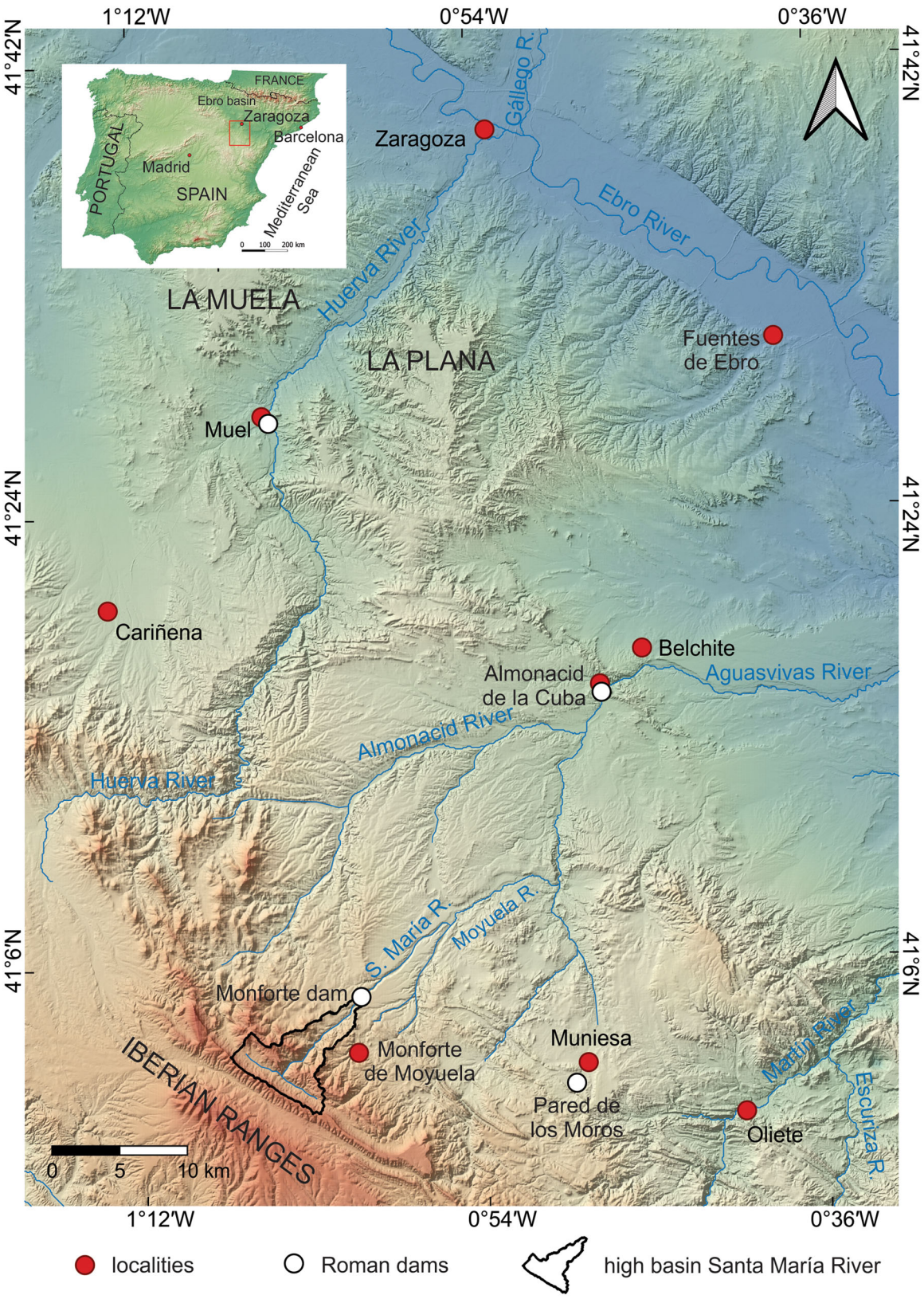

FIGURE 1 Location map of the Monforte de Moyuela dam and other Roman dams in the Huerva and Aguasvivas basins

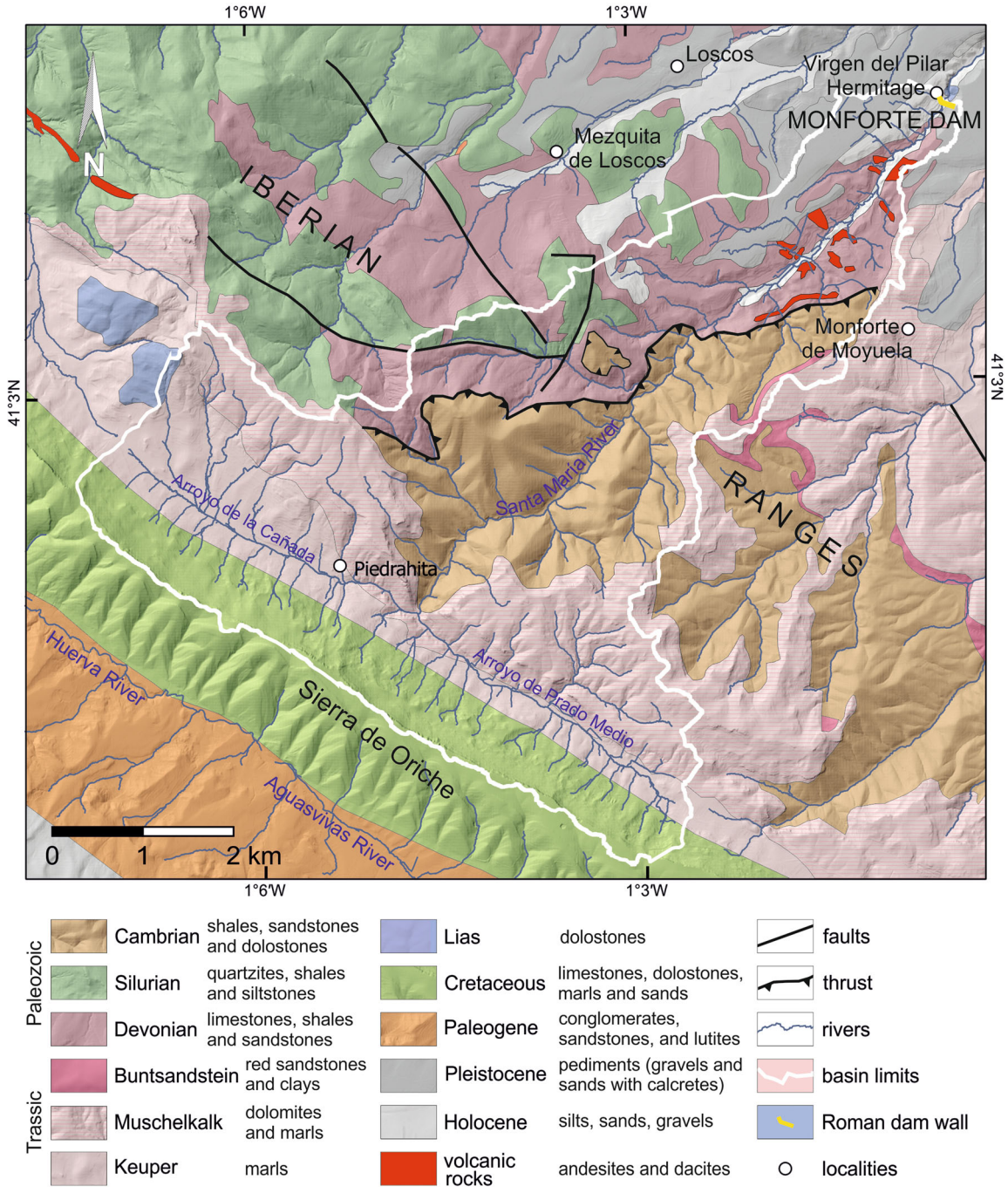

FIGURE 2 Geological map, with lithological units, of the upper section of the Santa María basin upstream of the Roman dam (reworked from the map of Ruiz Fernández de la Lopa & Carls, 1985).

dolostones (Muschelkak) and sandstones (Buntsandstein) of Monforte de Moyuela (Figure 2).

Erosive surfaces flatten a large extension of these geological units. Peña Monné et al. (1984) established that there are two large erosion surfaces on the central and eastern Iberian range: the "Intra-Miocene erosion surface" and the "Main erosion surface of the Iberian Ranges" of the Middle-Upper Pliocene age. The Intra-Miocene surface can be seen in several areas of the valley, partially covered with Miocene deposits, like in the Monforte dam area and the canyon located downstream (Figures 2 and 3), as well as the Moyuela area. The Main erosion surface is preserved in Sierra de Oriche, in the upper basin (Figure 2).

The last deformations of the Upper Pliocene uplifted these flattened mountainous massifs, favouring their erosion and promoting the formation of large pediments in contact with the Ebro depression. These pediments cover all previous geological structures. The upper margin of these antique Quaternary pediments is located in Mezquita de Loscos-Monforte de Moyuela area (Figure 2). They are formed by deposits that are often greater than

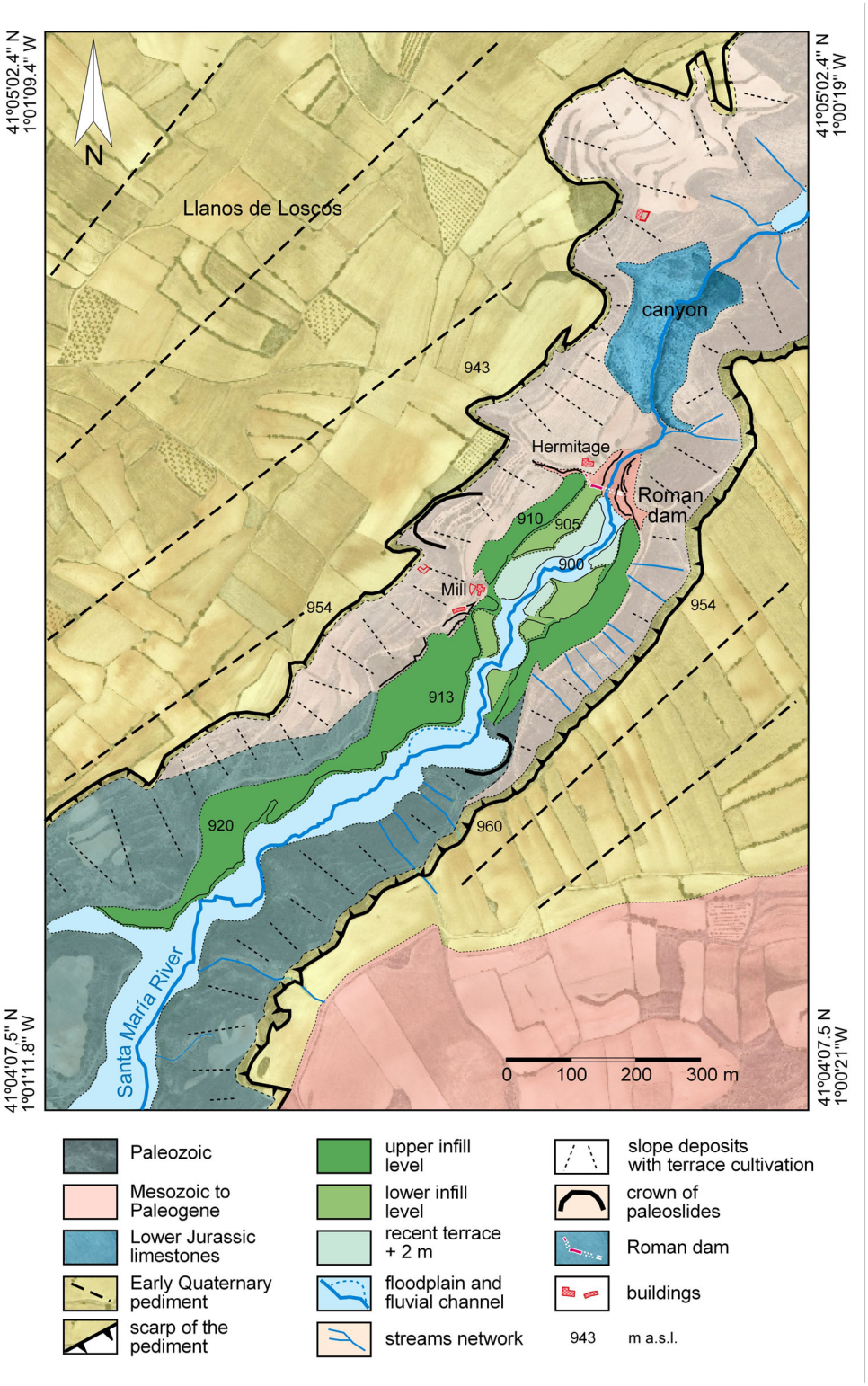

FIGURE 3 Geomorphological map of the Santa María River valley in the area of the Monforte dam

3 m in thickness, composed of sands and gravels with varied lithologies. Deposits are cemented with the development of superficial calcretes. The pediments possess a low gradient (around 2.5%) and are located about 800–900 masl.

Subsequently, the pediments were deeply excavated (between 40 and 60 m) by the Santa María River during the Quaternary, exhuming earlier geological units, visible throughout the interior of the valley. The Quaternary deposit hardness resulted in the

development of resistant corniches located on the incision top (Figure 3), promoting the formation of a relatively narrow valley. In general, these are low-resistance lithological units. However, there are limestones and dolostones from the Lower Jurassic (Lias) and Paleogene conglomerate outcrops crossed by the river forming deep canyons (Figure 3). One of these narrow sections was chosen to build the Monforte dam, as it provides a large upstream zone that collects water (Figure 2).

At present, the region is sparsely inhabited (mean population density of 1–3 inhab/km^2). The closest villages are Monforte de Moyuela (1008 m), Loscos (981 m), and Mezquita de Loscos (1020 m), which together have 250 inhabitants. The climate is continental with average rain of 300–350 mm per year (Peña Monné et al., 2002). There are more than 17 snow days per year, especially in the head basin (Sierra de Oriche, 1383 m). Snowmelt and the karstification of limestone areas located on the head basin allow constant river flow, although with marked shortages in the summer. The average flow of the Santa María River was estimated to be around 0.13 m^3/s (Arenillas et al., 2005).

3 | ARCHAEOLOGICAL CONTEXT

The study area lacks in-depth and systematic archaeological research. During the Second Iron Age (5th to 2nd century B.C.), it constituted a border zone between pre-Roman Celtiberian and Iberian peoples, centred on the Aguasvivas River. The best-known archaeological site is Los Castellares in Herrera de Los Navarros (Burillo, 1980, 2005) and those closest to the Monforte dam are Cabezo Aparicio or Samper (Simón, 1992); all are dated to the Bronze to Iron Ages.

During the Roman period, a series of secondary roads ran through this territory, connecting the lands of the Jiloca and Huerva rivers, with Aguasvivas and Ebro rivers. These roads would have been tributaries of two routes mentioned by the written sources. First, the road mentioned by the Antonine Itinerary (*It. Ant*. 446–448, Cuntz, 1929) from *Caesar Augusta* to *Laminio* (Fuenllana, Ciudad Real), one of the worst-known roads of the Iberian Peninsula (Magallón, 1987). Second, the road from *Contrebia Belaisca* (Botorrita, Zaragoza) to *Leonica* (Magallón, 1987), according to the Cosmography of Anonymous of Ravenna (IV, 43, Schnetz, 1940). Even though some of the Roman settlements cited in the written sources have not been recognized, other Roman archaeological sites, whose names remain unknown, have been documented. This is the case with the archaeological remains found at the Pueyo de Belchite site (2nd B.C. to 2nd century A.D.) (Rodríguez Simón & Díez de Pinos López, 2015). The urban center of the Pueyo de Belchite must have been supplied by the nearby Roman dam of Almonacid de la Cuba, with a chronology similar to that of the Monforte dam. In Late Antiquity, the Roman remains of the villa of La Malena in Azuara (Royo, 2010) stand out, with the main occupation between the 4th and 5th centuries A.D. (Royo, 1992).

The landscape changed during the Islamic civilization and made possible the installation and development of peasant communities located along the fertile alluvial terraces of the Aguasvivas River basin, which due to complex irrigation systems allowed intensive cultivation. The Muslim presence in the area was intense and has left place names such as as Nepza, Letux, Lagata or Azuara (Utrilla, 2010).

4 | METHODOLOGY

4.1 | Geomorphological mapping

Geomorphological mapping for the evolutionary reconstruction of the Monforte dam was undertaken using the orthoimage and DEM derived from SfM photogrammetry. These vertical aerial photographs were taken using the sUAV DJI Phantom 4 with an FC220 camera (12.4 Mpx) using a remote control equipped with an Android mobile device. A low-altitude flight (40 m) was preconfigured with Pix4D-Capture, and 220 photographs (80% overlapped) were taken in two perpendicular grids. The pictures were processed in Agisoft Metashape Professional v.1.5.1 to obtain an orthomosaic with a 2.36 cm/pix ground resolution and a DEM with a 4.72 cm/pix resolution. Three stereoscopic pairs were also used to improve cartographic details. For the graphical composition of the geomorphological map, QGIS v.3.12.2 was used, following the criteria proposed by Peña Monné (1997) for medium and detailed map scales.

4.2 | Geomorphological and archaeological fieldwork

Detailed pedestrian field surveys were conducted to locate all the remains of the Roman dam and establish the limits of the sedimentary fill. Other surveys were conducted along the inaccessible limestone canyon north of the dam, to locate remains of other constructions related to the dam and follow them to define their gradient and course. Finally, an archaeological survey was made in search of old buildings associated with the dam construction.

4.3 | Dam structure

Several *opus caementicium* mortar samples were taken to determine the different constructive units. The mineralogical composition was made by X-ray diffraction (XRD) analysis. The total sample was analysed by powder XRD on a PAN analytical X'Pert PRO X-ray diffractometer fitted with a Cu anode. Their operating conditions were 40 mA, 45 kV, divergence slit of 0.5°, and 0.5 mm reception slits. The samples were scanned with a step size of 0.0167° (2θ) and 150 ms per step. The samples were further characterized using the powder method between 5 and 60° (2θ). The specimens were quantified using Match v.3 and Fullprof software for Rietveld analysis (Rietveld, 1969; Rodriguez-Carvajal, 1993; Young, 1995). To identify

the phases present, the Crystallography Open Database (COD) reference standards were used. To know the clay minerals, a sample of oriented aggregates was prepared, studied with XRD analysis between 2/20°, and then quantified.

4.4 | Stratigraphic and pedological studies of the reservoir infill

Two stratigraphic columns were logged in the sedimentary fill of the Monforte dam, using the escarpments formed by the incision of the Santa María River. Magnetic susceptibility (in SI units) was measured (0.1 m analysis interval) using a KT-10 model susceptometer of Terraplus. Moreover, 14 samples were collected from the profiles for further study. For grain size analyses, an AMP0.40 W220 HZ59 CISA device with sieves of ¼ intervals between −1 and 4.75 Φ units was used. From the size distribution, a series of granulometric parameters were obtained using the software GRADISTAT (Blott & Pye, 2001). The carbonate content was estimated using a Geoservices manocalcimeter. The samples were analysed for determining the fossiliferous content. Finally, the percentages of the traction, saltation and suspension populations were calculated according to the methodology of Visher (1969).

Besides, in the pedological study, the sediment layers and soil horizons were described according to FAO guidelines (FAO, 2006). Organic carbon was determined by the wet oxidation method (Nelson & Sommers, 1982), and organic matter was calculated using the van Bemmelen factor (1.724).

4.5 | ^{14}C datings

Samples were taken to establish the chronology of the dam construction and the sedimentary infill of the reservoir. Small charcoal samples were found in the mortars, and they were used for the *opus caementicium* in two constructive units. As charcoals were scarce in the mortar core, we were not able to date all layers.

Besides, isolated charcoals, charcoal layers were also found in the stratigraphic and edaphic profile records from the infill. Two isolated charcoals were sampled in the lower section. Also, two levels with abundant micro and macrocharcoals were found in the upper section. They coincided stratigraphically with the base and top of the outcrop, allowing their dating. All samples were processed in the DirectAMS facilities and calibrated with Oxcal v4.4.4 (Reimer et al., 2020).

5 | RESULTS

Today the Santa María valley is 300–350 m wide in its upper conglomerate scarps and 35–40 m deep. It has cradle morphology with concave and relatively abrupt slopes reaching the flat valley floor. Only the Paleogene and Jurassic hard scarps break the general shape, forming two narrow sections, one of them in the Virgen del Pilar Hermitage and Monforte dam area. The sediments filling the interior of the reservoir during its activity period are preserved upstream of the dam along more than 1 km, giving a terraced shape to the valley floor (Figure 3).

5.1 | Dam structural characteristics and chronology

The Monforte dam is a gravity wall adapted to the irregular topography shaped by the river on the Paleogene conglomerates. It has a large initial wall, which was later increased in height (1 and 2 in Figure 4a–c). Along the first 6 m from the talweg at 896 masl, the channel forms a narrow V-shape (Figure 4). From 902 to 903 m, the gradient of the basal rock is gentler on the right margin, while the left one remains steep until 906–907 masl. The dam wall that closed the base of the canyon has disappeared completely. Only one sector is preserved—the one built above the middle step (902–903 masl), on the bedrock of the left margin (Figure 4a–c). From there, the wall reaches a height of slightly over 10 m up to the crest of the dam (Arenillas et al., 2005). Besides, there are a few remains of the wall extending towards the Virgen del Pilar Hermitage (3 in Figure 4c), as well as a small portion located on the right margin of the river, unknown to date (4 in Figure 4c).

At first sight, two overlying construction units can be identified (Figure 4a). The first-stage wall is located at an elevation of 910.20 masl, reaching a total height of 14.2 m, with large blocks and slabs on top. On this upper paving, a new wall of about 2.6 m was built. Therefore, the total height of the preserved wall is 16.8 m and its maximum length, which was initially 52 m, reached 86 m after it was heightened. Arenillas et al. (2005) provide a detailed description of the sizes and constructive system. The first-stage wall of the dam is a 6.9 m wide construction composed of a 4.3 m wide wall covered on the south side, upstream, by a 2.6 m wide panel attached to the water reservoir. This wall serves as a protecting panel for the core of the dam (Figure 5a).

The *main wall* is formed by a concrete core (B in Figure 5a,b) limited by two vertical masonry walls (A and C in Figure 5a,b). The ashlars of the walls were made of sandstone, microconglomerate and limestone. The ashlars on the internal wall are 85–90 m wide, while on the inner wall they are 60–65 cm wide. The ashlar construction facing downstream is relatively well preserved (C in Figure 5c), although weathered, and some ashlars were removed in the section closer to the hermitage. The inner ashlar wall is laterally covered by constructive unit D (Figure 5a), and its transversal profile is only visible in the broken wall facing the river (Figures 4a and 5b). The middle core (unit B) is formed by a 2.70–2.80 m mortar composed of strong *opus caementicium*, including blocks and boulders of different sizes, mainly limestones (Figure 5b,d).

In the *opus caementicium* of unit B, the contacts between the mortar layers are visible, and 15 layers of 50–55 cm in thickness were identified (Figure 5b). Two mortar samples were taken from layers B2 (sample PEP-B2) and B4 (sample PEP-B4) (Figure 5d) to determine their composition and compare them with other dam mortars. Both

FIGURE 4 Remains of the Monforte dam from (a) side; (b) front; and (c) overhead perspectives. Numbers represent the observed sectors: (1) original dam; (2) extended wall; (3) lateral extension and redirection and (4) remains from the right riverside.

samples are pink and the optical observations showed the predominance of siliceous rolled coarse sand. The mineralogical composition was evaluated by XRD (Figure 5e, Table 1a,b), which indicated prevailing quartz (71%) in PEP-B2, while PEP-B4 showed 49% gypsum, 35% quartz and 12% calcite. Gypsum is abundant in the basin (Keuper *facies* of the Upper Triassic). The lime:sand ratio is 1:19; the lime (including other sands):sand ratio is 1:1; and the lime:sand:gypsum ratio is 3:7:10 (Table 2). The mortar composition of the B4 layer was not observed in the other layers of the dam structure; however, it should be noted that it was not possible to obtain samples from the upper layers.

B layer of *opus caementicium* B was examined in detail, and two charcoal samples were obtained (Figure 5d). The lower one was collected 12 cm from the bedrock above which the wall was built (sample PEP-1), while the upper one was taken more than 2.1 m above the wall base (sample PEP-3) (Figure 5f,g). Some 8–10 mm charcoals were easily separated from the mortar. The dating (Table 3a) for PEP-1, after calibration (OxCal, Reimer et al., 2020), was 150–52 cal. B.C. (1σ)/174–43 (2σ). Sample PEP-3 dated to 42 cal. B.C.–22 cal. A.D. (1σ)/50 cal. B.C.–66 cal. A.D. (2σ).

A *protective wall* was attached to the main wall, upstream of the ashlars of unit C. The wall is formed by three units (Figures 5a and 6a). The inner unit (D) is composed of angular and rolled gravels with the large variability typical of the valley (quartzites, limestones, dolostone, volcanic rocks, shales, etc.), included in the pink mortar, as shown in Figure 6b. It forms a strong *opus caementicium*, over 1 m wide, in contact with the ashlars of unit C of the main wall. The central layer (unit C) is a 1 m thick *opus incertum*; it is badly cemented, so it is almost missing due to the removal of the ashlars of the next unit (F) (Figure 6a,c). Unit F is an *opus quadratum* built of parallelepiped ashlars, larger than the previous *opus incertum*, placed in horizontal isodomous rows, and sandstone/microconglomerate lithology with angular clast inclusions in the joints. This was the visible wall upstream, on the water reservoir side. Some ashlars remain at the west end of the dam (Figure 6a,c). They are well preserved and still have chisel marks (Figure 6d). Most of the original ashlars were re-used in the surrounding buildings, especially the Enmedio mill, located only 250 m away.

At present, most of the visible surface of the protective wall corresponds to the upper two-thirds of the *opus caementicium* of unit D (Figure 6a). The lower section remains covered with dam fill sediments. Unit D section is 3.5 m high, and six 50–55-cm-thick mortar layers (levels D1–D6) are separated by very well-defined discontinuities (Figure 6a). These can be used as constructive units. On top, there is the layer mentioned above, built with blocks and slabs, which was probably the upper layer of the initial dam (layer D7)

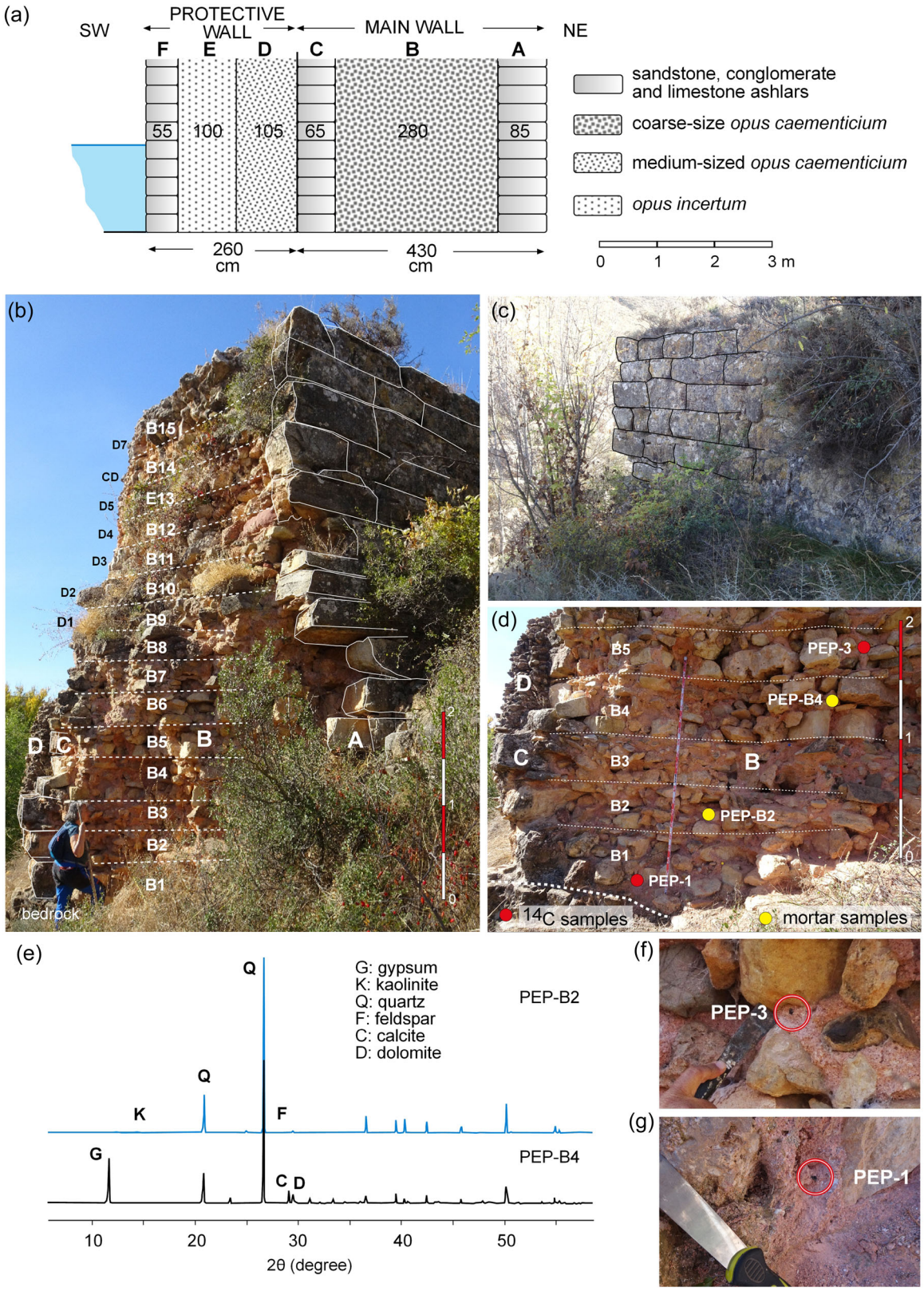

FIGURE 5 Original dam structure: (a) scheme of the constructive units and sizes; (b) interior of the main wall (units A, B, C), and layers of the *opus caementicium* of unit B; (c) ashlars of the frontal wall (unit A); (d) detail of unit B showing the mortar and charcoal sampling points; (e) PEP-B2 and PEP-B4 diffractograms; (f) and (g) details of the location of PEP-3 y PEP-1 charcoal samples.

TABLE 1 (a) Mineralogical composition by XRD of the mortar samples taken from the interior of the dam wall and (b) XRD patterns by phyllosilicate minerals for all the studied samples.

(a)								
Sample	**Quartz (%)**	**Feldspar (%)**	**Calcite (%)**	**Dolomite (%)**	**Phyllosilicates (%)**	**Gypsum (%)**	**Thenardite (%)**	**Dam sector and level**
PEP-G2	10	n.d.	42	5	40	1	1	Increased wall G2
PEP-G1	15	n.d.	37	5	22	11	10	Increased wall G1
PEP-D6	38	n.d.	52	Traces	7	3	n.d.	Initial wall E6
PEP-D4	71	n.d.	11	Traces	12	6	n.d.	Initial wall E4
PEP-D3	68	n.d.	11	Traces	14	7	n.d.	Initial wall E3
PEP-D2	71	n.d.	4	n.d.	22	n.d.	n.d.	Initial wall E2
PEP-D1	69	n.d.	9	4	12	6	n.d.	Initial wall E1
PEP-X	38	n.d.	58	4	Traces	n.d.	n.d.	Rigth bank
PEP-B4	35	n.d.	12	4	n.d.	49	n.d.	Initial wall B4
PEP-B2	71	16	3	Traces	10	n.d.	n.d.	Initial wall B2
PEP-X2	10	n.d.	90	n.d.	Traces	n.d.	n.d.	Channel downstream

(b)			
Sample	**Kaolinite (%)**	**Smectite (%)**	**Chlorite (%)**
PEP-G2	60	40	n.d.
PEP-G1	70	30	1
PEP-D6	100	n.d.	n.d.
PEP-D4	100	n.d.	n.d.
PEP-D3	100	n.d.	n.d.
PEP-D2	100	n.d.	n.d.
PEP-D1	100	n.d.	n.d.
PEP-X	Traces	n.d.	n.d.
PEP-B4	n.d.	n.d.	n.d.
PEP-B2	100	n.d.	n.d.
PEP-X2	Traces	Traces	n.d.

Abbreviation: n.d., not detected; XRD, X-ray diffraction.

(Figure 6a). Some inner layers, like D2, have particular features, where whitish limestone angular clasts from the Jurassic are dominant, in contrast to the other darker layers. Also, the base of the D4 layer is formed by dark greenish dacitic rocks (Figure 6b) coming from nearby outcrops.

Samples from D1 (PEP-D1), D2 (PEP-D2), D3 (PEP-D3), D4 (PEP-D4) and the base of D5-6 (PEP-D6) mortar layers were taken. XRD results are shown in Figure 6e and Table 1a,b. Samples PEP-D1 to PEP-D4 show the same mineralogical distribution, with 68%–71%, quartz 4%–12% calcite and a similar presence of kaolinite. The ratio between aggregates is also similar, between 5% and 10% of CaO. Besides, the lime:sand ratio is 1:19; the lime (including other sands):sand ratio is 1:4 and the lime:sand:gypsum ratio is 3:14:3 (Table 2). However, sample PEP-D6 shows some mineralogical changes. Calcite increases (52%), quartz (38%) diminishes (Table 1a; Figure 6e) and CaO reaches 30%. The ratios of lime:sand (3:5) and lime:sand:gypsum (3:5:2) also change (Table 2). Besides, the mineralogical composition of PEP-D6 coincides with that obtained for the PEP-X sample taken in the residual mortar from the other river side (Figure 6f,g). This is probably because they belong to the same constructive unit. Layer D7, formed by large slates, is not only on the protective wall top but also on the principal wall forming a generally flat surface. Although the mortars of units A–E and X were examined, no charcoal fragment was found, and therefore, we do not have absolute datings for the protective wall.

The *extended wall* was built on the roof of the first dam (unit G). It is, at least, 2.6 m high, and four layers (G1–G4) made of *opus caementicium* were identified (Figures 6a and 7a). Thus, the dam length increased from 52–53 m to 86–87 m. Besides, the dam front is at least 16.8 m in height (Arenillas et al., 2005), although the water reservoir must have been relatively filled with sediments. The lateral expansion of the reservoir occurred mainly on the left side, so the wall was extended at an angle of 50° (3 in

TABLE 2 Ratios among the main components of the mortar samples

Sample	CaO (%)	Lime:sand	Lime (other salts included):sand	Lime:sand:gypsum	Dam sector and level
PEP-G2	25		1 to 1	25:50:25 = 1:2:1	Increased wall G2
PEP-G1	25		1 to 1	25:50:25 = 1:2:1	Increased wall G1
PEP-D6	30		3 to 5	30:50:20 = 3:5:2	Initial wall E6
PEP-D4	10		1 to 4	15:70:15 = 3:14:3	Initial wall E4
PEP-D3	10		1 to 4	15:70:15 = 3:14:3	Initial wall E3
PEP-D2	5	1:19			Initial wall E2
PEP-D1	5		1 to 4	15:70:15 = 3:14:3	Initial wall E1
PEP-X	32	2:3			Rigth bank
PEP-B4	6		1 to1	15:35:50 = 3:7:10	Initial wall B4
PEP-B2	5	1:19			Initial wall B2
PEP-X2	50	1:1			Channel downstream

TABLE 3 (a) ^{14}C datings from the mortars of the dam structure and (b) ^{14}C datings obtained from the sedimentary fill (radiocarbon ages were calibrated with Oxcal v. 4.3 over the IntCal 20 curve (Reimer et al., 2020) and expressed with 1σ and 2σ).

(a) Dam						
Sample	**Lab. code**	**^{14}C B.P.**	**Cal. B.P. (1σ)**	**Cal. B.P. (2σ)**	**Cal. B.C./A.D. (1σ)**	**Cal. B.C./A.D. (2σ)**
PEP-1	D-AMS 039801	2092 ± 24	2099–2001	2123–1992	150–52 B.C.	174–43 B.C.
PEP-3	D-AMS 039802	2012 ± 22	1991–1928	1999–1885	42 B.C.–22 A.D.	50 B.C.–66 A.D.
PEP-4	D-AMS 039803	1895 ± 29	1829–1745	1881–1727	122–206 A.D.	69–223 A.D.
(b) Sedimentary fill						
Sample	**Lab. code**	**^{14}C B.P.**	**Cal. B.P. (1σ)**	**Cal. B.P. (2σ)**	**Cal. B.C./A.D. (1σ)**	**Cal B.C./A.D. (2σ)**
RPEP-6	D-AMS 042658	3366 ± 24	3637–3566	3689–3493	1688–1617 B.C.	1740–1544 B.C.
RPEP-5	D-AMS 0044699	3795 ± 24	4234–4099	4245–4089	2285–2150 B.C.	2296–2140 B.C.
RPEP-3	D-AMS 039804	1781 ± 22	1710–1625	1724–1610	240–325 A.D.	227–341 A.D.
RPEP-7	D-AMS 043096	1468 ± 21	1370–1312	1382–1307	580–639 A.D.	568–644 A.D.

Figure 4), almost until the present-day Hermitage (Figure 7b). At the dam abutment, the extended wall is attached to a scarp of Paleogene conglomerates. The extended sector is highly degraded, with only a small remaining sector because it was partially removed a few years ago to widen the path to the agricultural field. Their remains are large concrete blocks lying on the nearby slope (Figure 7c).

The extended wall is formed by two *opus caementicium* constructions (Figure 7a) composed mainly of limestone boulders and other lithologies from the nearby area included in a whitish mortar. The intermediate fill has almost disappeared. Its complete thickness could have been similar to the set of walls of the previously built dam, although it is not possible to confirm this because the external ashlars were removed. Arenillas et al. (2005) suggest that the wall facing the reservoir may have been stepped, although there is no evidence pointing to that. Two mortar samples were taken from this upper wall: Unit G1 (PEP-G1) and unit G2 (PEP-G2) (Figure 6a). Their mineralogy is shown in diffractograms (Figure 7e) and Table 1. Both samples differ greatly from those of the original dam wall. They show a higher percentage of phyllosilicates (22%–40%, with chlorite, smectite and kaolinite) and calcite (37%–42%), containing 22% OCa (Table 1b). The lime (including other salts):sand ratio is 1:1 and the lime:sand:gypsum ratio is 1:2:1 (Table 1b).

The mortar of unit G1 shows many charcoal fragments of millimetric size. A 6 mm charcoal fragment was selected (PEP-4) (Figure 7d) and dated to 122–206 cal. A.D. (1σ)/69–223 cal. A.D. (2σ).

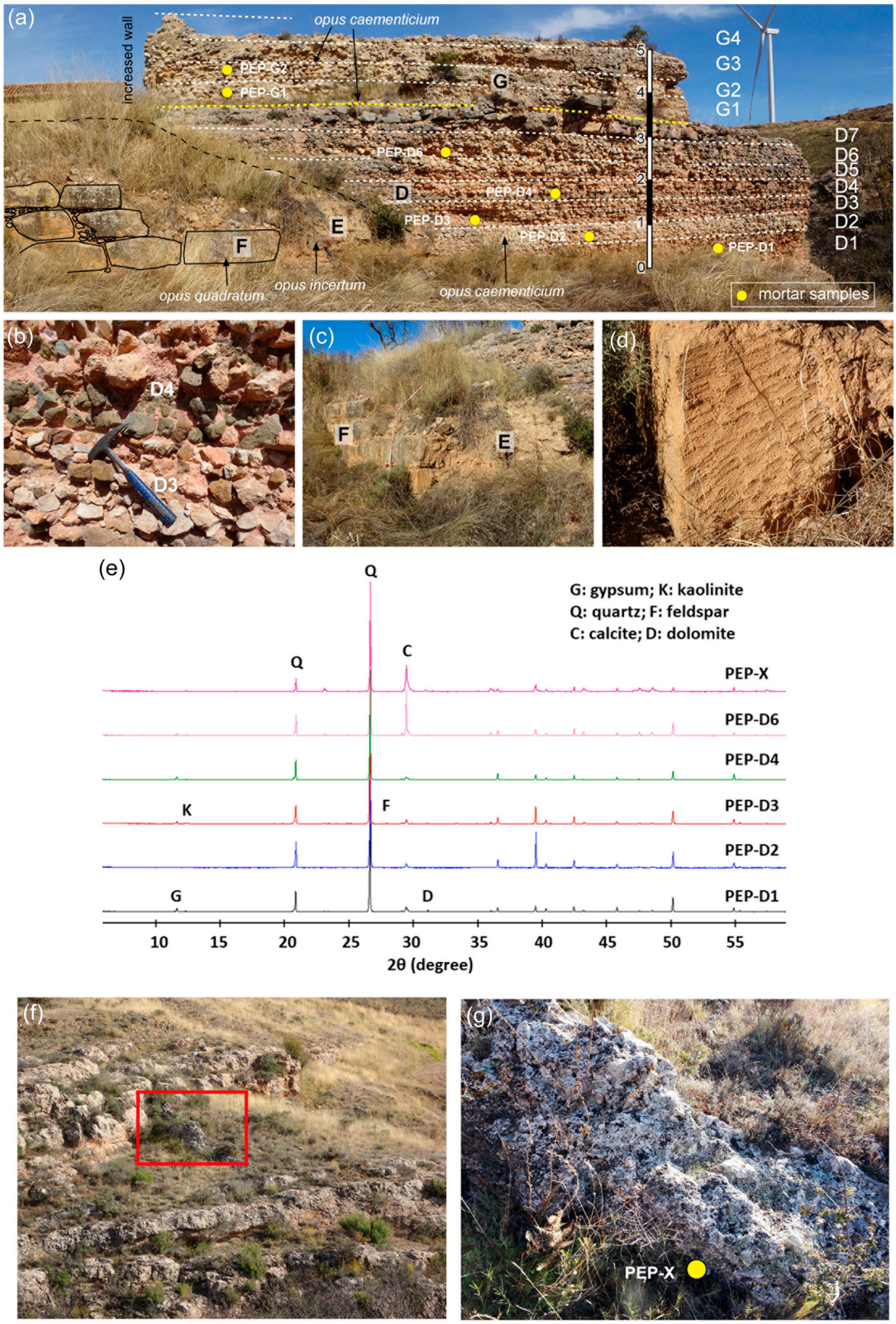

FIGURE 6 Original dam structure: (a) units of the initial wall (units D, E, F), and increased wall (unit G), with layers of the *opus caementicium* and the location of the mortar sampling points; (b) detail of the composition of unit D; (c) ashlars remaining from unit F and poorly consolidated gravel fill of unit E; (d) carving marks of an ashlar from unit F; (e) diffractograms of mortar samples from different layers of unit D; (f) location of mortar remains located on the right riverside; (g) detail of the mortar from the right riverside and the location of the PEP-X sample.

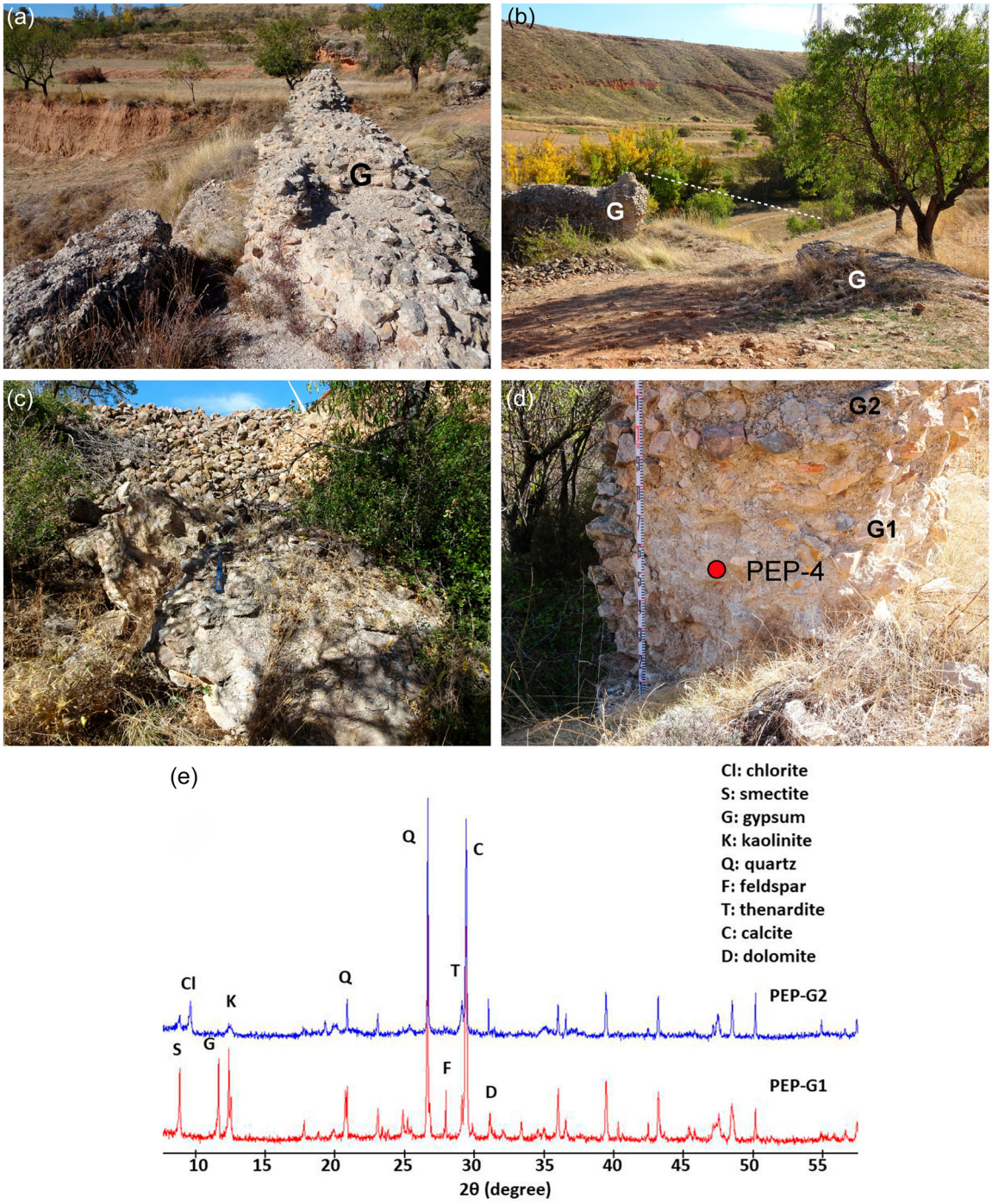

FIGURE 7 Dam extended wall: (a) *opus caementicium* of the central sector of the dam in the increased section (unit G, subunits G3 and G4); (b) western closing of the wall increase, partially removed to open a path; (c) remains of the *opus caementicium* removed from the wall located in a nearby slope; (d) subunit G1 of the wall extended and the location of the charcoal PEP-4 sample.

5.2 | Other construction remains

The archaeological survey brought to light scattered remains of possible water conduits related to the dam. One of them is located 150 m downstream of the dam, about 5–6 m above the river channel, on a rocky ledge at the entrance of the limestone canyon (Estrecho de la Virgen del Pilar). It is a small isolated construction formed by large limestone and conglomerate fragments included in a hard mortar (Figure 8a). There is a cavity at its base, bordered by large vertical limestone blocks and covered with well-carved and vaulted tufa ashlar (Figure 8b). This structure belonged to a water conduit whose length is still unknown. There are notches and grooves in the

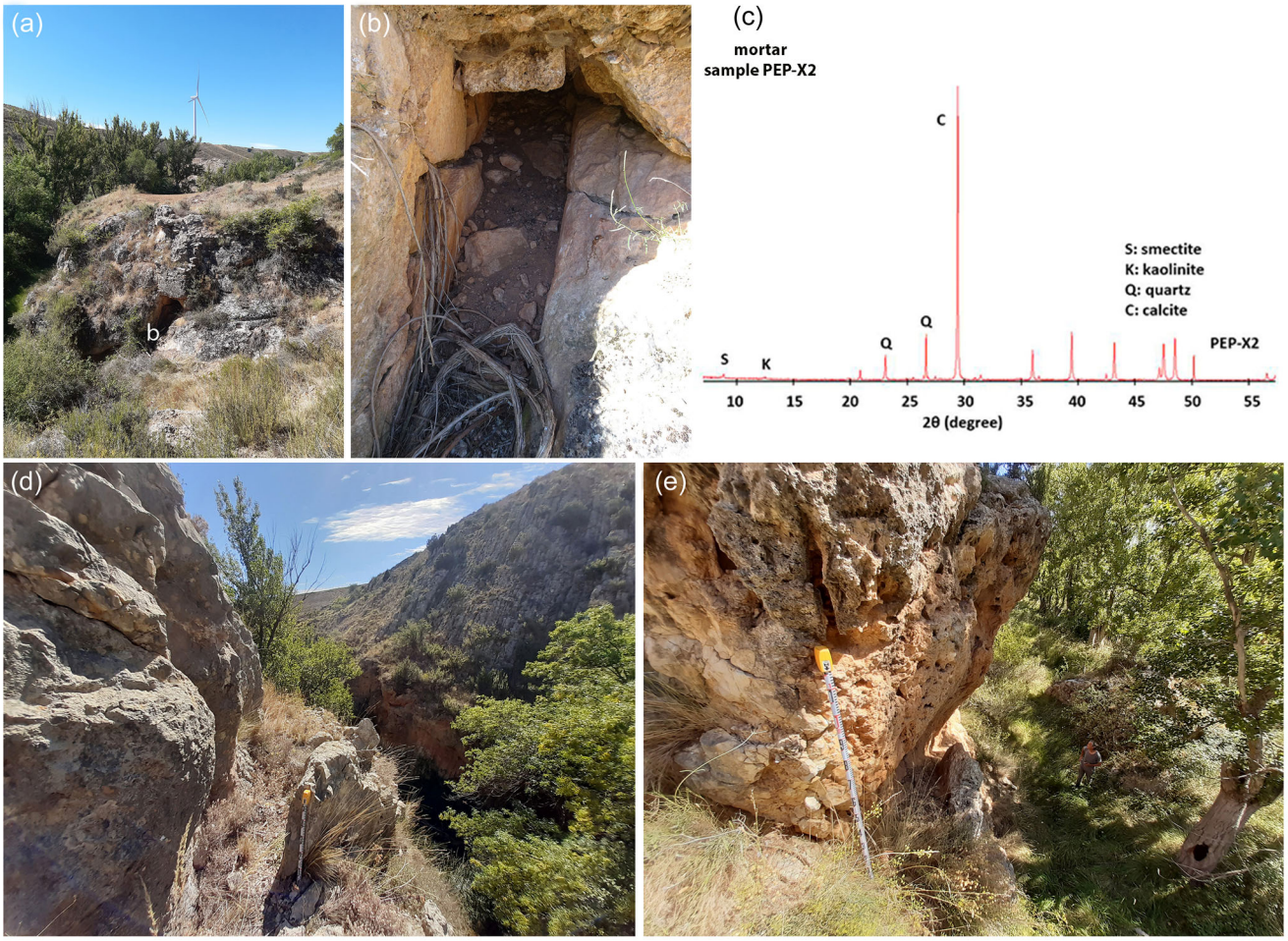

FIGURE 8 Remains of water conduits: (a) wall and conduit outlet; (b) detail of a well-preserved section; (c) diffractogram of the mortar from the water conduit (sample PEP-X2); (d) channel section in the limestone canyon; (e) canal carved on the limestone tuffs at the end of the canyon.

rock probably related to floodgates used for directing flow. One mortar sample (PEP-X2) of this structure was analysed (Figure 8c, Table 1). The diffractogram shows a large calcite (90%) proportion in its composition and the lime:sand ratio is 1:1 (Table 2). This mortar differs greatly from the ones used in both phases of the dam construction. The most similar samples (Table 1) are PEP-X and PEP-D6 from the upper part of the protection wall, due to the higher carbonate content. This may be due to the fact that the canal was constructed after the dam and the second wall were built, but we do not have enough data to confirm this.

At this point, a narrow limestone canyon begins. Over the last third of this feature, there are several undercuts carved in the rock, representing the remains of a much eroded antique irrigation ditch (Figure 8d). The best-preserved undercut was opened on the Quaternary tufa located at one end of the canyon (350 m away from the dam). It still has vertical sides carved along a continuous stretch (Figure 8e). Future surveys may reveal other remains of this water conduit downstream toward Moyuela and provide more information about the use of the reservoir.

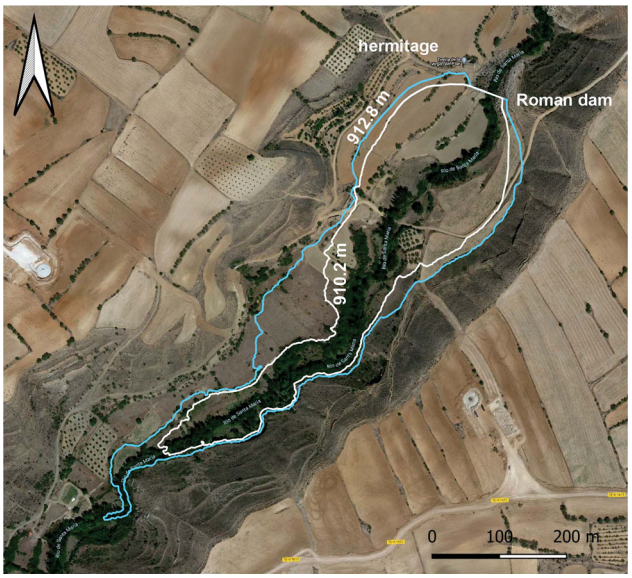

FIGURE 9 Contour of the estimated water reservoirs. Original dam at 910.2 masl and after the construction of the extended wall at 912.9 masl.

5.3 | The reservoir and its sedimentary record

The dam reservoir occupied a large area (~120 m maximum width), narrowing toward the tail located around 770–790 m away from the Monforte dam (Figure 9). The initial altitude level of the wall was calculated at 910.2 masl and that of the second wall at 912.80 masl (as the minimum known), according to Arenillas et al. (2005). This allowed us to estimate a reservoir surface of between 81,237 m^2 (in the first construction) and 111,480 m^2 (after the second construction), increasing its surface by 25% (Figure 9). This expansion could have meant a notable increase in the availability of water, but part of the reservoir was already full of sediments up to 905 or 906 masl as we will show in the stratigraphical analysis. It is difficult to estimate the volume of the reservoir. Arenillas et al. (2005) estimated 280,000 m^3 for the first construction and almost twice as much for the second one, although they subtracted 100,000 m^3 as the filling value.

Two stepped accumulations of sediments were found upstream of the dam walls, above the Paleogene outcrop (Figure 3). The largest and oldest accumulations (upper and lower infill levels) are the sedimentary record corresponding to the operating times of the reservoir. Besides, there are more recent sediment deposits, forming after the dam collapse.

The preservation of the sedimentary fill forming two steps can be interpreted in several ways, which may only be resolved by detailed geomorphological, stratigraphic, chronological and edaphic studies. These steps allowed us to differentiate a lower unit and an upper unit, which we used in our analysis. These two levels are especially well-defined in the area near the dam wall, in both river margins up to the mill (Figures 3 and 10a). They are better developed and have visible outcrops on the right riverside (Figure 10b). The two stratigraphic sections, with a total sedimentary thickness of 7.9 m (4.15 m for the lower section and 3.75 m for the upper one), were divided into six units (A–F) according to lithological and sedimentological features (Figure 11, Table 4) and magnetic susceptibility (Table 5).

5.3.1 | Lower section

Unit A: This is a 2.1-m-thick unit consisting of dark grey marly silts with abundant ochre discolourations. It exhibits massive texture and columnar habit. Silts include scattered, rounded clasts of up to 3 cm in diameter, root bioturbation and crusted stems. Two channelized beds are interbedded in the marly silts. They are 30 and 10 cm thick and composed of gravels and massive or laminated sands in fining-upward sequences. The unit contains abundant remains of gastropods, ostracods, charophytes and charcoal. Unit A requires a low-energy environment where suspended sediments have time to settle. Sand and gravel intercalations are related to water discharge of erosive pulses within a slack water environment. This unit corresponds to the Roman period of the main

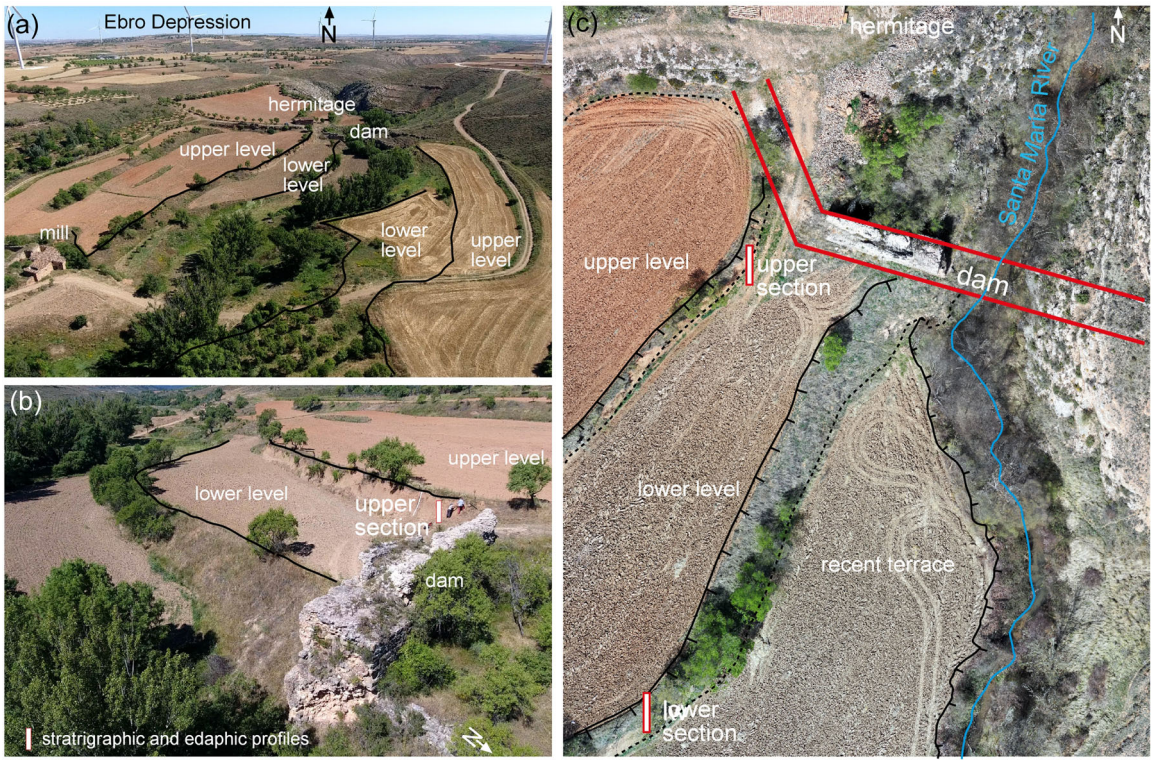

FIGURE 10 Different aerial views from (a) south; (b) east; and (c) overhead of the two steps of the sedimentary fill from the Monforte dam and the location of the two analysed profiles

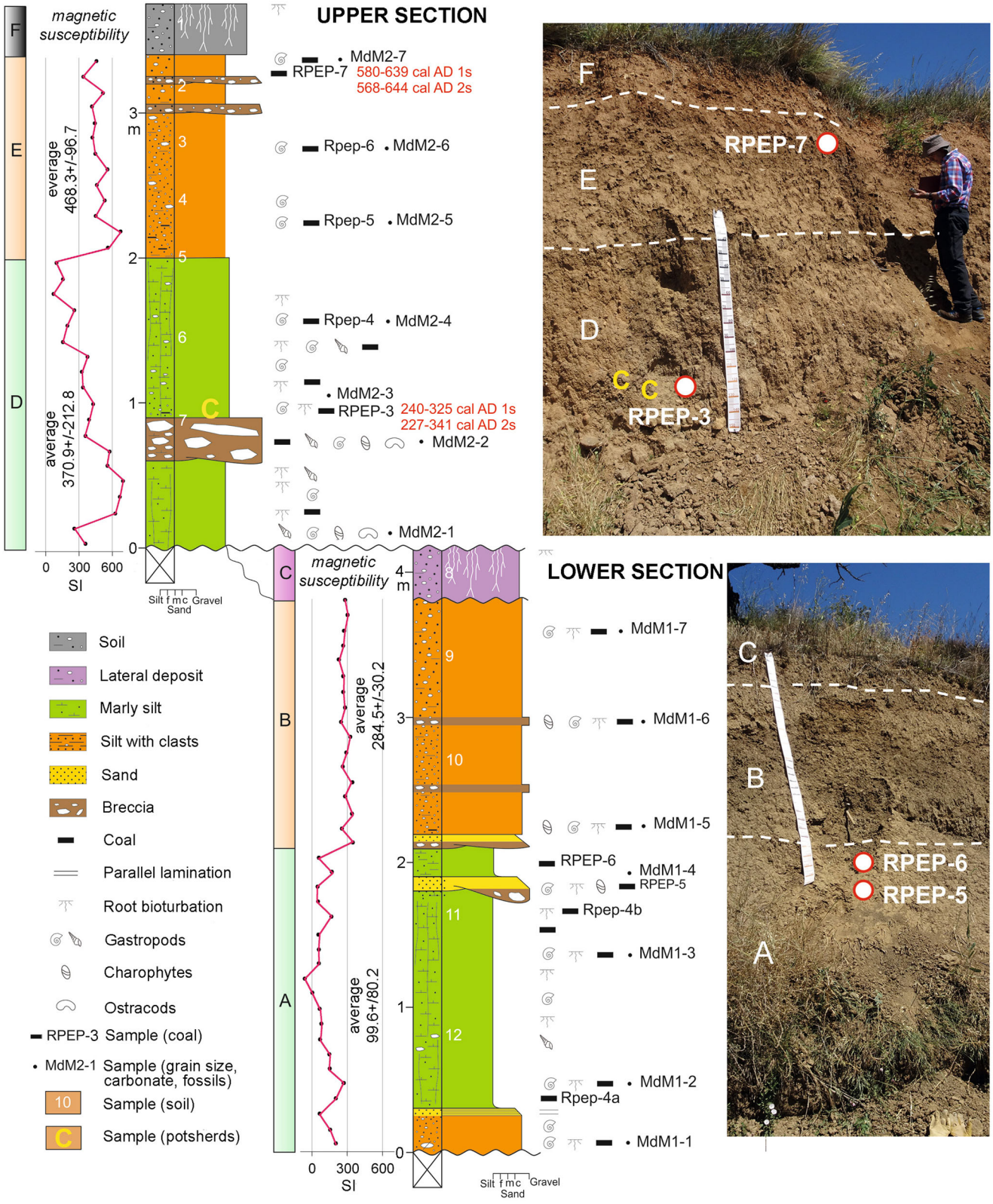

FIGURE 11 Stratigraphic units of the sedimentary fill of the Monforte dam. Morphologically, the lower and upper sections correspond to the two stepped levels of the reservoir fill.

TABLE 4 Granulometric parameters of the sedimentary infill samples of the Monforte dam

Sample	Unit	Gravel (%)	Sand (%)	Silt + Clay (%)	Mean (μm)	Traction (%)	Saltation (%)	Suspension (%)	$CO_3^=$ (%)
Upper section									
MdM2-7	E	2.4	14.2	83.4	295.7	0.0	4.0	96.0	15
MdM2-6	E	0.2	14.3	85.5	163.9	0.0	0.0	100	9
MdM2-5	E	0.4	12.6	87.0	149.1	0.0	0.5	99.5	7
MdM2-4	D	0.8	7.0	92.2	237.8	0.0	0.0	100	8
MdM2-3	D	0.9	12.1	87.0	187.1	0.0	0.0	100	20
MdM2-2	D	0.1	13.8	86.1	191.2	0.1	3.0	96.9	20
MdM2-1	D	0.0	5.0	95.0	170.9	0.0	1.0	99.0	8
Lower section									
MdM1-7	B	4.6	16.1	79.3	550.5	0.0	8.0	92.0	10
MdM1-6	B	2.6	14.4	83.0	446.1	0.0	7.0	93.0	12
MdM1-5	B	9.1	46.5	44.4	449.1	0.0	16.0	84.0	10
MdM1-4	A	7.0	35.8	57.2	1007.0	0.0	32.0	68.0	10
MdM1-3	A	2.0	10.6	87.4	382.4	0.0	3.0	97.0	8
MdM1-2	A	0.5	13.5	86.0	156.2	0.0	2.0	98.0	5
MdM1-1	A	1.2	11.7	87.1	284.0	0.0	3.0	97.0	7

Note: Silt + clay is the dominant size in all samples except for the sandy MdM1-5. The samples are poorly sorted with mean sizes between 149.1 and 1007 μm. Transport was carried out mainly in suspension, by settling down within a slack water environment. Carbonate content is low, corresponding to a siliceous source area.

Monforte reservoir activity. Two charcoal samples were taken from the upper part of unit A (Figure 11). Sample RPEP-5, in a lower position (1.75 m), was dated to 2285–2150 cal. B.C. (1σ)/2296–2140 cal. B.C. (2σ), while sample RPEP-6 (located 0.20 m above) was dated to 1688–1617 cal. B.C. (1σ)/1740–1544 cal. B.C. (2σ) (Table 3b). These datings do not have absolute chronological value but point to the post-quem age. However, they show the abundance of paleo-fires in the basin before the Roman Epoch.

Unit B: This is a 1.7-m-thick unit consisting of massive brown silts with abundantly scattered clasts (<1 cm diameter) and tabular and channelized gravel beds, with clasts up to 5 cm. They include gastropods, charophytes, root bioturbation and coal remains. This unit was formed in areas temporarily occupied by a sheet of water where erosive streams carried silt and gravel. Unit B may be related to the dam-filling stage (Figures 12b and 13b).

Unit C: This is a 0.35-m-thick unit characterized by massive brown silts with abundantly scattered clasts and root bioturbation. Unit C is interpreted as a colluvial deposit affected by agricultural labour.

Magnetic susceptibility measurements in the lower section show very different values for A and B units: Unit A: $99.6E^{-6}$ (SI) and a standard deviation of 80; unit B: $284.5E^{-6}$ (SI) and a standard deviation of 30.2 (Table 5; Figure 11). This change in the magnetic susceptibility points to the existence of two different stages in the filling of the reservoir corresponding to periods of activity (unit A) and inactivity (unit B) of the Monforte dam.

5.3.2 | Upper section

Unit D: This is a 2-m-thick unit composed of grey-ochre marly silts with ochre discolourations. The silts exhibit massive texture and include scattered clasts, up to 5 cm in diameter. The root bioturbation and crusted stems are abundant in the lower part. The unit contains abundant remains of gastropods, ostracods, charophytes and coal, mainly in the lower part. A gravel channelized bed, 30 cm in thickness, is interbedded in the marly silts. Unit D may correspond to a new period of dam activity after the wall extension. One charcoal sample was taken (RPEP-3, unit D), at 1 m profile height (Figure 11), and it was dated to 240–325 cal. A.D. (1σ)/227–341 cal. A.D. (2σ) (Table 3b). This charcoal-rich layer also included four fragments of Roman pottery. These ceramic finds are fragments of common cooking ware, with rough-textured clay bodies without surface treatment, of presumed local manufacture. Therefore, they are inconclusive types and cannot be used to reinforce the chronology accuracy.

Unit E: This is a 1.4-m-thick unit made of ochre massive silts with scattered clasts (<15 cm in diameter). The silts include scarce gastropods and coal remains. There are two channelized gravel beds in the upper part. Unit E may be related to the second dam filling stage (Figures 12d and 13d). A charcoal sample (RPEP-7) was taken from the top of unit E, at a profile height of 3.35 m (Figure 11), and it was dated to 580–639 cal. A.D. (1σ)/568–644 cal. A.D. (2σ) (Table 3b).

TABLE 5 Magnetic susceptibility measurements (SI) in the lower and upper sections of the sedimentary infill of the Monforte dam

LOWER SECTION			
	Depth (cm)	SI	Average (SI)
UNIT B	370	288.3	284.5 ± 30.2
	360	298.0	
	350	271.7	
	340	277.3	
	330	219.0	
	320	260.0	
	310	277.0	
	300	297.3	
	290	258.3	
	280	315.0	
	270	294.3	
	260	256.7	
	250	336.3	
	240	292.3	
	230	317.3	
	220	252.3	
	210	325.7	
UNIT A	200	73.7	99.6±80.2
	190	181.3	
	180	51.3	
	170	56.3	
	160	153.3	
	150	42.0	
	140	57.3	
	130	46.0	
	120	−75.3	
	110	−1.0	
	100	62.7	
	90	86.0	
	80	78.3	
	70	152.0	
	60	151.0	
	50	265.7	
	40	202.7	
	30	65.0	
	20	141.0	
	10	202.0	

TABLE 5 (Continued)

UPPER SECTION			
	Depth (cm)	SI	Average (SI)
UNIT E	320	342.3	468.3 ± 96.7
	310	310-0	
	300	508.7	
	290	407.0	
	280	431.7	
	270	429.0	
	260	432.3	
	250	567.3	
	240	471-0	
	230	516.3	
	220	441.7	
	210	669-o	
	200	561.7	
UNIT D	190	101.7	370.9±212.8
	180	147.0	
	170	74.0	
	160	254.3	
	150	200.0	
	140	149.0	
	130	378.3	
	120	311.3	
	110	334.7	
	100	411.7	
	90	393.3	
	80	369.3	
	70	574.0	
	60	549.0	
	50	881.0	
	40	668,3	
	30	636.0	
	20	256.7	
	10	358.0	

Unit F: This is a 35-cm-thick unit characterized by massive brown silts with abundantly scattered clasts and root bioturbation. Unit F is interpreted as soil.

Magnetic susceptibility measurements in the upper section also show very different values for D and E units: Unit D: $370.9E^{-6}$ (SI)

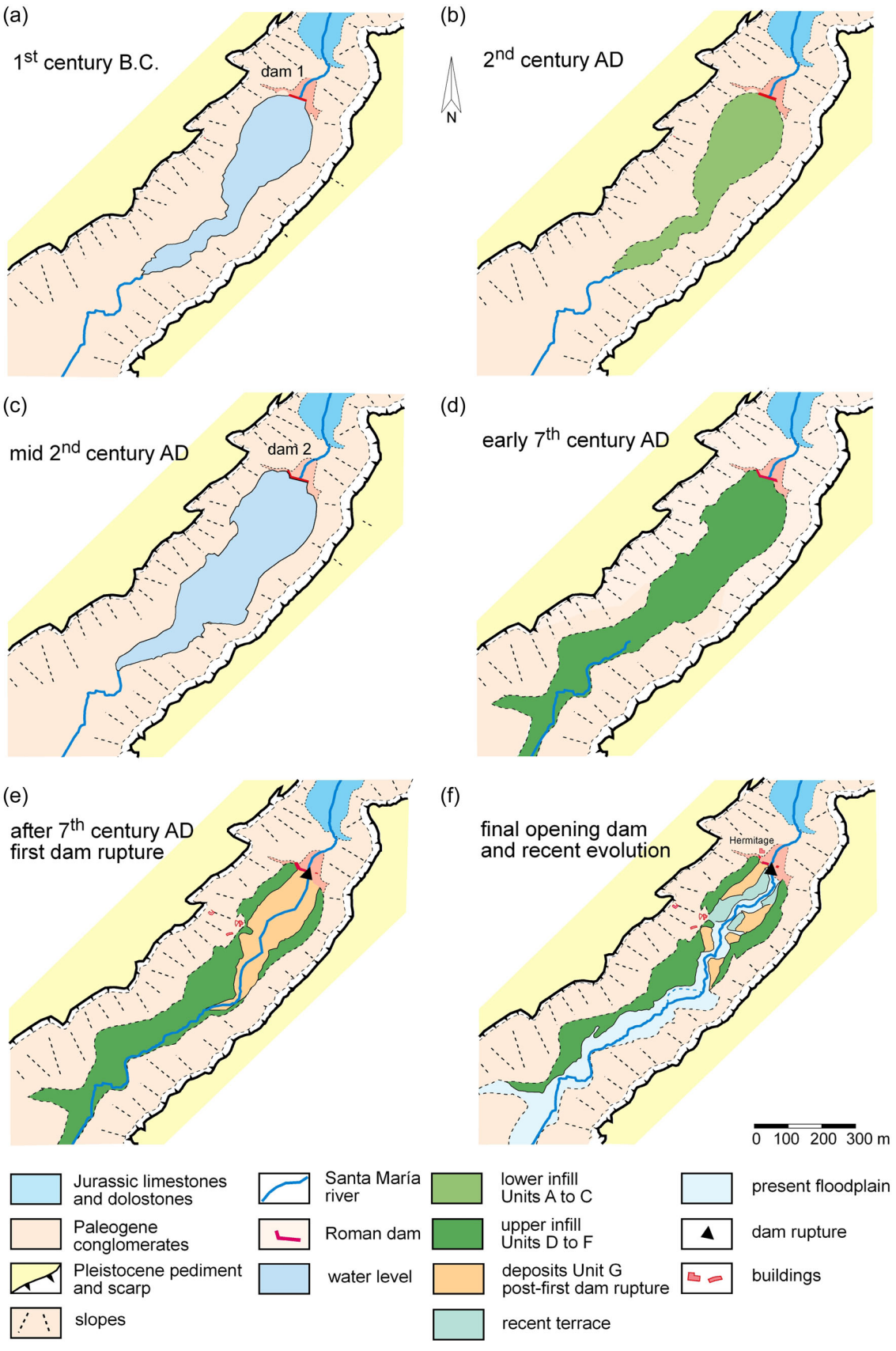

FIGURE 12 Evolutionary scheme of the sedimentary fills from the Monforte dam: (a) construction of the first dam during the 1st century B.C.; (b) siltation of the reservoir before the 2nd century A.D.; (c) extended wall, 2nd century A.D.; (d) reservoir filled in the 7th century A.D.; (e) wall breaking and partial emptying of sediments, after 7th century A.D.; (f) final opening and general incision of the sedimentary fill.

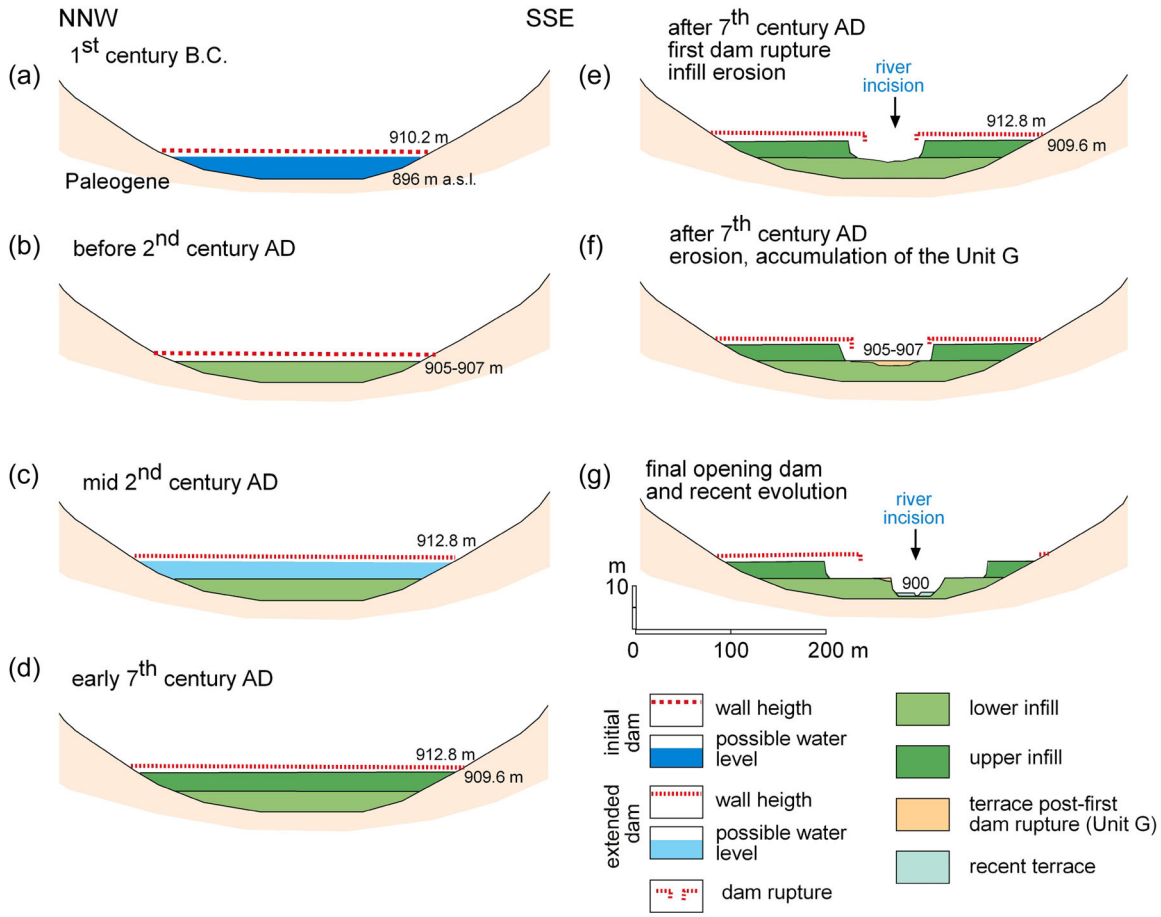

FIGURE 13 Evolutionary cross sections of the sedimentary fills of the Monforte dam: (a) initial dam, 1st century B.C.; (b) siltation before the 2nd century A.D.; (c) extended wall, 2nd century A.D.; (d) reservoir fill, 7th century A.D.; (e) wall breaking; (f) partial emptying of sediments, accumulation of the Unit G (terrace), after 7th century A.D.; (g) final opening, incision and recent evolution.

and a standard deviation of 212.8; unit E: 468.3E^{-6} (SI) and a standard deviation of 96.7 (Table 5; Figure 11). As in the lower section, two stages were detected in the magnetic susceptibility. They represent the accumulation during the activity (Unit D) and inactivity (E) periods of the extended Monforte dam.

Unit G: This unit is separated from the profiles analysed. It was formed after the first wall rupture and the filling of the upper section was partially eroded. It is discordantly sedimented in the lower section. Unit G is composed of a mix of fluvial deposits and materials eroded from the upper units. It is a small terrace because it was deeply eroded after the dam totally collapsed.

5.4 | Edaphic analysis of the sedimentary fill

In addition to stratigraphic records and analyses, the morphological description of the soil and underlying sediments was carried out, by focusing on unit F. This is an interesting unit because it is located on top of the fill and was exposed for at least the last 1400 years. Besides, it was necessary to determine whether the other units contained edaphic anomalies like unit C. Unit F is the transition between the two fill sections of the reservoir, formed by a lateral deposit affected by agricultural activity.

The upper unit (F) corresponds to young, poorly developed soil, with a reddish yellow colour (7.5 YR 6/6) when dry and strong brown (7.5 YR 4/6) when wet (Table 6). It has many coarse fragments (>2 mm), from fine to coarse gravel measuring 2–60 mm, polygenic in nature and subrounded (tabular or flat) in shape; some of the fragments have calcium carbonate coatings without a defined distribution in the clasts, which evidence their origin from eroded soils from the upper pediment surface. The soil is strongly calcareous (10%–25%, w/w), with its maximum on the surface and without morphological evidence of secondary or edaphic carbonates, as a result of its youth. The organic matter content is maximum in this unit (around 2%, w/w) and decreases progressively with depth. This is a demonstration of certain soil development or edaphization that is not observed at greater depth (Table 6). The soil structure, moderately developed, is fine and granular in the topsoil, turning into subangular blocky and medium-sized with depth. In the topsoil, very few fine-sized roots can be found. In addition to the bioturbation caused by roots, the presence of earthworm channels, some of them empty, others full of worm casts, is remarkable. In the 85 superficial cm, we did not find gastropod shells, which appear

TABLE 6 Main pedofeatures and components of the studied units

	Upper section							
Sedimentol. Units	**F**	**F**	**E**	**E**	**ED**	**D**	**D**	**Slope**
Pedolog. samples	**1**	**2**	**3**	**4**	**5**	**6**	**7**	**-**
Thickness (cm)	0–25	25–85	85–140	140–200	200–270	270–320	320–400	400–500
Coarse elements (%, v/v)	30	30	<2	<2	10	<2	<2	
Charcoal (%, v/v)	-	-	2	5	1	1	-	
Shells (%, v/v)	-	-	2	-	-	5	10	
Mottles	-	-	-	-	-	-	+	
Other								
Organic matter (%, w/w)	2.13	1.48	1.13	1.01	0.94	1.11	1.34	
Hue (Munsell) dry	7.5YR	7.5YR	10YR	10YR	10YR	10YR	10YR	
Value (Munsell) dry	6	6	6	6	6	6	7	
Chroma (Munsell) dry	6	6	4	4	4	3	2	
Munsell colour (dry)	reddish yellow			light yellowish brown		pale brown	light grey	

	Lower section					
Sedimentol. Units	**C**		**B**	**B**	**A2**	**A1**
Pedolog. samples	**8**		**9**	**10**	**11**	**12**
Thickness (cm)	500–590		590–650	650–700	700–750	750–800
Coarse elements (%, v/v)	10		<2	<2	10	<2
Charcoal (%, v/v)	-		-	-	-	-
Shells (%, v/v)	5		5	5	-	1
Mottles	+		++	++	++	+++
Other					Coarse sand	
Organic matter (%, w/w)	1.18		1.23	0.89	0.47	0.81
Hue (Munsell) dry	7.5YR	10YR	10YR	10YR	10YR	10YR
Value (Munsell) dry	6	5	6	6	6	6
Chroma (Munsell) dry	4	1	3	3	4	3
Munsell colour (dry)	light brown	grey	pale brown		light brown	pale brown

only at greater depths (unit E), at the limit of the lithic discontinuity. This is not the only change detected, since at depth the sediment turns brown and grey. Thus, unit E is light yellowish brown (10YR 6/4, dry) and dark yellowish brown (10YR 4/4, wet), according to the Munsell colour chart, and has practically no stones. This unit has a prismatic structure, and it is common to observe charcoal, which is also present at greater depths. In addition, the organic matter content in unit E drops to half that of the topsoil. This value, with slight fluctuations (which correlates with the texture of the sediment), is maintained up to 8 m.

In unit D, a greyer layer appears at 320–400 cm depth; specifically, it is light grey (10YR 7/2) when dry and brown (10YR 5/3) when wet, and more snail shells were found (Table 6, sample 7); moreover, this layer is slightly richer in organic matter (1.34%) than the top and bottom layers. It is in this layer that mottles begin to appear and continue throughout the remaining units of the lower part. The RPEP-3 charcoal sample dated to ^{14}C comes from layer 7 (Table 3a) and also contains fragments of Roman pottery (Figure 11). Specifically, fine-sized mottles are abundant in the second part (units C, B and A), and their presence increases with depth. They indicate that the sediments, usually under wetting conditions (reducing), had some local oxidizing conditions (in fauna channels and root pores). These mottles can be contrasted (with a 5YR hue in a sediment matrix with a 10YR hue, both when dry), and they increase their presence with depth: there are few (5% v/v) in unit C; some (5–15% v/v) in unit B and many (15–40%) in unit A (Table 6).

6 | DISCUSSION

A general evolutionary framework can be established from the different proxies used in the study of the Monforte dam. To achieve this objective, it is necessary to discuss and assess each proxy in the following order: first, the chronological data provided by the mortars

of the dam wall and the sedimentary fills of the reservoir; second, the linkage of the sedimentary fills with the regional paleoenvironmental framework and finally, the dam breakage process and its later geomorphological evolution.

6.1 | Chronology of the dam construction

There are several possible chronological frameworks for the dam's construction, each with different levels of precision, relating to constructive styles, types of materials and mortars. These characteristics, among others, are normally used to establish the age of Roman constructions (Barahona, 2018a). In the first study of the Monforte dam, Arenillas et al. (2005) applied constructive criteria (size and materials) to establish the dam chronology. They proposed that "by its typology, this dam is probably one of the first dams built in Hispania (1st century AD)". Considering that there are Roman constructive elements (ashlars' size and shape, type of mortar, structural arrangements) that were also used in later constructions or repairs (like those in the Proserpina dam, Feijoo, 2005, 2006), the constructive criteria can induce to chronological errors. In other cases, an attempt was made to use the inscriptions on the ashlars as a chronological feature, like the case of the Muel dam (Uribe et al., 2016), to no avail. Besides, organic remains in the stratigraphy of the reservoir fills are datable, if they are accessible, giving information about the chronology of different layers and the useful life of the dam. In this case, the ages correspond to times after theconstruction of the dam wall and the oldest are found at the base of the profile, being closer in age to the construction of the dam. Sometimes, it is difficult to know how much time elapsed between wall construction and sedimentation; even older charcoals can be found, eroded from accumulations from the surroundings and washed into the reservoir. Isolated charcoals found on the profile may raise concerns about age reliability; however, due to their abundance, it is possible to achieve higher chronological accuracy. In several cases, they originated from fires in the basin and can yield information about deforestation and erosion.

However, the most accurate chronology is provided by the dating of the materials from the dam wall construction. Thus, the lime mortars can contain chronological information. Many studies obtained ^{14}C absolute ages using carbonated mortars but the results have large standard deviations in datings (Hajdas et al., 2012, 2017; Hayen et al., 2019; Lubritto et al., 2018; Ringbom et al., 2014). Similar results are obtained by using luminescence (OSL) (Urbanová & Guibert, 2015, 2017). The organic remains (small twigs, leaves, charcoal fragments) of the dams are difficult to find but very useful for dating. Two wood fragments were collected from the foundations of the walls of the Almonacid de la Cuba dam (Arenillas, 2002). In the case of the Monforte dam, all visible mortar sectors were intensively surveyed in search of organic remains to carry out radiocarbon datings of the different constructive layers, as if they were stratigraphic units. No charcoal was found either in the wide sector of the protective wall (units D, E and F) (Figure 6a), in the small remnant of the mortar located on the right side (Figure 6g) or in the marginal units of the main wall (units A and C). However, two samples—8–10 mm charcoal fragments—were selected from the *opus caementicium* fill (unit B), accessible on the river cut (Figure 5d) (samples PEP-1 and PEP-3; Figures 5f,g). Also, the extended wall (unit G) (Figure 7d) contained many small fragments in the mortar (sample PEP-4).

The three calibrated ages obtained by ^{14}C are chronologically consistent from the base to the top of the wall. Sample PEP-1, located only 12 cm above the rock in the middle section of the wall, yielded the earliest age: 150–52 cal. B.C. (1σ)/174–43 cal. B.C. (2σ) (Table 3a). PEP-3 sample, 2 m high, dated to 42 cal. B.C.–22 cal. A.D. (1σ)/50 cal. B.C.–66 cal. A.D. (2σ) (Table 3a). The most plausible date is the younger one; thus, the construction of the dam wall began between 50 B.C. and 66 A.D., probably coinciding with the time of Emperor Augustus, like other nearby dams (e.g., Muel and Almonacid de la Cuba dams). At present, the height between the rock under the wall and the talweg of the Santa María River is about 5 m. As the riverbed is so deep, if we consider the preserved wall base, we may infer that there were other earlier constructive layers and that the wall construction began even before those dates. Finally, the last sample, PEP-4 (subunit 1G) from the base of the extended wall (unit G) was dated to 122–206 cal. A.D. (1σ)/69–223 cal A.D. (2σ) (Table 3a). Thus, the extended wall was probably built in the second half of the 2nd century A.D.

As well as the chronological information, the composition of the *opus caementicium* is useful to identify constructive styles and building phases (Ahmad Bany Yaseen et al., 2013; Drdácký et al., 2013; Miriello et al., 2010). However, there are no studies on the composition and mixtures of these concretes in dams. In the Monforte dam, there are several differences in the composition of the mortars of the initial dam wall and the extended wall section, in addition to the time that elapsed between their ages. Samples PEP-G1 and PEP-G2 have more calcitic composition than the samples from units B and D (Table 1a); kaolinite prevails among the phyllosilicates (Table 1b); there are only limestone fragments in the *opus caementicum*. There are also notable differences in the lime:sand:gypsum ratios (Table 2). In particular, there are differences in the same parameters if samples PEP-D6 (higher part of the original wall) and PEP-X (remains of the dam on the right bank of the river) are compared with the rest of the original wall. It is possible to infer that the mortar composition changed by the end of the construction of the initial wall and this is more notable in the extended wall. As we pointed out above, the sample taken from the water conduit (PEP-X2) is also of the calcitic type, more similar to the extended wall mortar, although with a different composition. Hence, from the constructive point of view, four types of mortars can be identified: two on the original wall, one on the extended wall and one on the remains of the water conduction. It is not possible to compare the mortars from Monforte with other dams because there are no equivalent studies to date.

6.2 | Reservoir fill and regional environmental conditions

In many sedimentary fills of antique reservoirs, since the stratigraphy is not accessible, mechanical drilling is used to obtain samples for radiometric dating or archaeomagnetic stratigraphy. This is the case with the Muel dam (Pueyo et al., 2008; Silva Aguilera et al., 2008) and Almonacid de la Cuba dam (Arenillas, 2002; Pueyo et al., 2001). It is also possible to carry out excavations to access the complete stratigraphy and perform sequential sampling for radiocarbon dating, as in the case of the Muel dam (Uribe et al., 2012). However, at the Monforte dam, these activities were favoured by the natural cut made by the river after the wall rupture. The incision allowed us to observe a natural outcrop with two steps, showing a total profile of 7.9 m (Figures 10c and 11). The cleaning of these outcrops in search of internal structures and edaphic interbedding allowed us to find charcoal samples. It was not possible to drill under the profile to reach the base of the lower section (Unit A) and complete the sedimentary sequence because access was difficult and permissions were not obtained.

The lower samples taken from the lower section (RPEP-5 and RPEP-6) of unit A yielded earlier ages than expected for Roman dams 2296–2140 cal. B.C. (2σ) and 1740–1544 cal. B.C. (2σ), respectively (Table 3b). There were no other samples with enough organic matter in the section. We believe that these isolated charcoals in the deposit are the result of previous fires produced on the slopes of the valleys and washed downslope. The obtained datings belong to the Late Neolithic and Early Bronze Ages, coinciding with regional deforestation processes (Peña Monné, 2018). These datings are earlier than dam construction so they were not included in Figure 11.

Besides, two other ^{14}C datings were made from the upper section of the fill outcrop (Figure 11; Table 3b). These charcoal samples are more reliable because they are not isolated fragments but sedimentary layers with horizontal continuity. Even one of them, where RPEP-3 was taken, also contained Roman potsherds. The data suggest fast and sort-distance transportation of the materials. The first (RPEP-3), taken at a height of 1 m from the base of unit D, was dated to 240–325 cal. A.D. (1σ)/227–341 cal. A.D. (2σ); the second (RPEP-7), located on the upper section of unit E, was dated to 580–639 cal. A.D. (1σ)/568–644 cal. A.D. (2σ). These two dates are consistent with the datings from subunit G1 (PEP-4) of the extended wall (Figure 7d; Table 3a).

The other two large reservoirs from the Aguasvivas basin ages are similar to ours. Only the foundation age of the Almonacid de la Cuba dam is known (Arenillas, 2002). The ^{14}C results were calibrated to 167 cal. B.C.–116 cal. A.D. (2σ) and 94 cal. B.C.–204 cal. A.D. (2σ), but the final fill ages are not known. In the case of the Muel dam (Huerva River), the sediment base was dated to 170 cal. B.C.–50 cal. A.D. (2σ) and the reservoir siltation to around the 4th century (249–426 cal. A.D. [2σ]) (Uribe et al., 2012), and it was not extended after that. In summary, the three dams have average dates of construction around the second part of the 1st century B.C. Radiocarbon dates include the Epoch of Emperor Augustus and confirm the archaeological studies. Siltation ages vary between the 4th century for the Muel dam and the middle of the 2nd century for the Monforte dam. The Monforte dam is the only one that was subsequently increased in height, which shows that the purpose for which it was created was still valid.

In the outcrops of Figure 11, it can be seen that the sedimentary sequence of the initial and extended dams began with sediments from the flooded environment during the activity of the Monforte dam (units A and D). In both cases, they were covered with debris deposits from the runoff (units B and E) produced during the times when the dam was no longer active. The curve of the magnetic susceptibility shows the same pattern (Table 5, Figure 11). In the lower section, unit A (deposited in the active reservoir) seems to have few magnetic minerals with 99.6 (SI), in contrast to unit B (produced by runoff transport) with inherited magnetic minerals showing 284.5 (SI). In the upper section, unit D (flooded) has 370.9 (SI), higher than the lower section infills (units A and B) but lower than unit E (runoff), the last one with 468.3 (SI). In general, magnetic susceptibility values increase as the reservoir fills, showing the increment of detritic materials supplied by the surroundings, from the dam construction to the final infill. As we will see, higher detritic availability might be related to land use changes during Roman Epoch.

It is difficult to establish the sedimentation rates of the lower section since we do not have datings from the base of the visible fill. Also, it is important to note that the base of the lower section (901 masl) is 4–5 m above the base of the dam wall (896 masl). Thus, it is possible to estimate another 4–5 m of fill in the unseen part of the deposit. Accordingly, taking the PEP-1 sample as the starting age of the sedimentation (100 cal. B.C.–10 A.D.) and the end of the dam filling at the beginning of the wall extension (PEP-4, around 150 cal. A.D.), the accumulation rate would be around 3.6 m/century. For the upper section, the estimation is made based on more accurate dates, starting around 150 A.D. and ending by 600 A.D. Sedimentation rates for this upper section would be of ca. 0.7 m/century, although the reservoir was wider than the previous one and, therefore, the sediment volume could be similar to that of the lower section. It is possible to estimate a rate of about 1.7 m/century for the complete infill, around 12 m including the unseen part. The continuity of the filling process is confirmed by the contents of organic matter (MO) (about 1% in weight) up to 7 m in depth, except in the sandy channels. Similarly, the rates estimated for the fillings of the Muel dam are about 1–2 m/century (Pueyo et al., 2008; Silva Aguilera et al., 2008).

The Monforte dam was constructed under favourable climatic conditions, during the Roman Climate Optimum (RCO), also named the Roman Warm Period (RWP). This period greatly favoured Roman expansion across the Mediterranean. Chronologically, this period elapsed between ca. 200 B.C. and 150 A.D. (Harper &

McCormick, 2018; McCormick et al., 2012). Warm and relatively dry conditions are reflected in some lakes in the Iberian Peninsula, such as the Zoñar lake (Martín-Puertas et al., 2008) between 190 B.C. and 150 A.D., and in the tufa records from the central sector of the Peninsula between 175 cal. B.C. and 160 A.D. (Currás et al., 2012). Likewise, these conditions are observed in the coastal hinterland of Emporion, according to the recent study of Ejarque et al. (2022).

Deforestation in the Mediterranean region began before the Roman Epoch. However, it is the expansion of agricultural activity at that time that caused the greatest loss of vegetation and the main changes in the landscape (Luterbacher et al., 2012). Some authors (Reale and Dirmeyer, 2000; Reale and Shukla, 2000) argue that Roman deforestation is one of the factors determining the dryness of the current Mediterranean climate due to the decrease in plant evapotranspiration and soil loss due to erosion (Dümenil-Gates and Liess, 2001). The studies of historical aggradation/degradation processes occurring in the central sector of the Ebro basin show the influence of deforestation and soil overexploitation during Roman times and especially during the Late Roman Epoch (Constante et al., 2010; Peña Monné, 2018; Peña-Monné et al., 2004). The same tendencies were pointed out by Dusar et al. (2011) and Notebaert et al. (2014) in other Mediterranean regions. In fact, the construction and operation of Roman dams are contemporary to the greatest erosive degradation. Peña-Monné and Sampietro-Vattuone (2019) estimated erosion rates of about 4.5 m/1000 years in the valley of the central Ebro depression during such a period. For this reason, all Roman reservoirs were usually filled in a few centuries, losing their utility and being abandoned. In the Ebro basin, only the Almonacid de la Cuba dam (Aguasvivas River) and the Monforte dam (Santa María River) were enlarged to ensure their functionality. At present, the former is still operating as a water diversion weir, although filled up. Another large construction, the Muel dam (Huerva River) was filled around the 4th century (249–426 cal. A.D. [2σ]) (Uribe et al., 2012) and was not subsequently increased in height.

6.3 | Dam rupture and the erosion of the fill

The upper section of the sedimentary fill of the Monforte dam ended, after the most recent date (ca. 5th century A.D.), with lateral deposits and poorly developed soil (Figures 12d and 13d). After that, the centre and eastern area of the dam wall collapsed. In our opinion, the wall did not collapse up to its base but it was a partial breach (Figures 12e and 13e). This is supported by the fact that only a part of the upper section of the filling was eroded, while the lower section was retained, giving rise to the development of a new valley floor in coincidence with the contact between both sections (Figure 12e). In addition, near the dam wall, the lower section lost unit B and part of unit A, which were replaced by a new accumulation (unit G in Figures 12e and 13f), showing a continuous terrace level at that height. At the same time, the upper unit scarp retreated laterally (Figures 12e and 13f). In no other way could the formation of the two steps showing both sections have occurred. Vertical aerial photographs taken in 1946 and 1956 were reviewed to determine whether the steps could have been a consequence of recent flattening works. However, the stepped morphology already existed at that time. The western side of the dam wall was not affected because its base lies on Paleogene conglomerates, favouring its conservation up to the present. Finally, sometime later, the river canyon was completely open and headwater erosion formed the current course of the Santa María River (Figures 12f and 13g). According to Arenillas et al. (2005), the dam collapsed due to a lack of stability in the construction, especially after the wall was extended, because the relationship between wall thickness and height is not adequate. However, the reservoir remained closed for more than four centuries after being increased in height and operated up to its final siltation. Some large flows may have overpassed the wall on its eastern side, causing part of it to crumble. The most recent evolution formed a flat fill, 2 m in height, on the riverbed, probably due to a temporary closure of the incision (Figure 3). This surface is located near the narrowing of the canyon and it is part of the floodplain.

It is not possible to infer a dam management system because there are no gates or spillways. There are only a few conduits, as shown, about 100 m below the dam wall. The structure was probably used to provide water for irrigation of the Santa María valley. There is no information about Roman city mills, small populations in the surroundings, or Roman *villae* that would allow us to speculate about another type of water use. In any case, it is necessary to intensify the surveys, especially in the lower section of the Santa María River, to fully understand the construction and maintenance effort of this water reservoir for many centuries.

7 | CONCLUSIONS

The Monforte dam is part of the set of hydraulic works built during the Roman period during the reign of Augustus in the Aguasvivas and Huerva river basins, both tributaries of the Ebro River. Its construction could have been the result of Augustus' new territorial organization, which unfolded during his reign with the promotion of the *municipia*, the foundation of a new colony, *Caesar Augusta*, and the creation of its road network. As the dam wall collapsed after Roman times, it was possible to observe, record and sample the wall interior and most of the sediment fills of the reservoir, allowing an interdisciplinary study. The dam is composed of an initial wall, built between 50 BC and 66 AD. Later, the dam wall was increased in height in the mid-2nd century. The analyses of the *opus caementicium* mortars allowed us to establish differences between these constructive phases. The initial wall has a siliceous composition, while the extended wall is carbonatic. They also differ in the lime:sand:gypsum ratios. The sedimentary study of the reservoir fill shows the sequences of activity and silting of both stages, reflected by deposit composition and changes in the magnetic susceptibility measurements. The first reservoir was silted before the mid-2nd century and the enlarged reservoir was built in the early 7th century (609–606

A.D.). No paleosoils are interbedded in the fill and the organic matter content is constant, showing the lack of sedimentary interruptions. There is an exception in a level dated to ca. 3rd century A.D., with higher organic matter content and roman potsherds.

The siltation of the reservoir was rapid as a consequence of the intense erosion in the basin, promoted by intense anthropic impact by land use change during the Roman Epoch. The accumulation rate was estimated at 1.7 m/century. Subsequently, the dam broke in two phases, which first gave rise to erosive steps in the fill and then the emptying of the central sector.

Some construction remains are related to water conduction downstream of the dam, probably built for agricultural irrigation in the lower valley of the Santa María River. This dam, barely known due to its location, deserves to be a properly preserved and valued site of interest, which would enable visitors to appreciate its construction and the natural setting in which it is located.

ACKNOWLEDGEMENTS

This work is warmly dedicated to the authors' friend and colleague Arsenio Muñoz, who passed away during the review process of this article. His collaboration with the sedimentological description of the dam infill is a fundamental part of this study. The authors would like to thank Mr. Bernardino Herrera, owner of the fields where the dam is located, for allowing them to perform the sampling. They also thank the support of the Mayoress and the Secretary of the City Council of Monforte de Moyuela for facilitating their procedures. They are grateful for the help of Ana Paula Conte and Silvia Quintana, Universa students, who collaborated with the sampling; they are equally grateful to Fernando Pérez Lambán, Javier Fanlo and Marta Espinalt for the survey throughout the canyon and to Carlos Mazo for allowing them to use the drone orthoimage in one figure. This research was carried out with the support of ANPCyT (PICT2018-1119; PICT2019-0931). Several ^{14}C datings were financed by the IUCA (Instituto Universitario de Investigación en Ciencias Ambientales de Aragón). P. Uribe worked on this paper through the post-doctoral contract "Beatriz Galindo" (BEAGAL 18/00191 Agencia Estatal de Investigación de España-Universidad de Zaragoza). Finally, they appreciate the observations made by the reviewers to improve the publication.

ORCID

José Luis Peña-Monné http://orcid.org/0000-0003-4067-8222
María Marta Sampietro-Vattuone http://orcid.org/0000-0002-7681-070X
Uribe Agudo Paula http://orcid.org/0000-0001-8911-0393
María Ángeles Magallón Botaya http://orcid.org/0000-0001-7713-7126

REFERENCES

Ahmad Bany Yaseen, I., Al-Amoush, H., Al-Farajat, M., & Mayyas, A. (2013). Petrography and mineralogy of Roman mortars from buildings of the ancient city of Jerash, Jordan. *Construction and Building Materials*, *38*, 465–471.

Álvarez Martínez, J. M. (2007). El agua de Augusta Emerita. In J. Mangas, & S. Martínez (Eds.), *El agua y las ciudades romanas* (pp. 183–212). Ediciones Madrid.

Álvarez Martínez, J. M., Nogales, T., Rodríguez Martín, F. G., & Gorges, J. G. (2002). Arqueología de las presas romanas de España: Los embalses de Emerita Augusta y de sus alrededores. Estado de la cuestión. In F. Bueno (Ed.), *Actas del I Congreso Nacional de Historia de las presas* (pp. 199–226). Editorial Universitaria.

Aranda, F., Carrobles, J., & Isabel, J. L. (1997). *El sistema hidráulico romano de abastecimiento a Toledo*. Instituto Provincial de Investigaciones y Estudios Toledanos.

Aranda, F., Sánchez Carcaboso, J. L., Andrés, E., Rodríguez Martín, F. G., Polo, M. E., Sánchez Crespo, R., & Gutiérrez Gallego, J. A. (2006). *Las presas de abastecimiento en el marco de la ingeniería hidráulica romana*. Los casos de Proserpina y Cornalvo [PDF file]. http://www.traianvs.net

Aranda, F., & Sánchez Carcaboso, J. S. (2000). Las grandes desconocidas entre las presas romanas principales: La Alcantarilla y Cornalbo. In F. Bueno (Ed.), *Actas I Congreso de Historia de las Presas* (Vol. I, pp. 267–278).Universidad Complutense de Madrid.

Arenillas, M. (2002). *La presa romana de Almonacid de la Cuba y otros aprovechamientos de la época romana en la cuenca del río Aguasvivas*. Estudio técnico de los aprovechamientos. [PDF file]. http://www.traianvs.net/almonacid/almona01.htm

Arenillas, M. (2003). Presas romanas en España. *Ingeniería y Territorio*, *62*, 73–79.

Arenillas, M., & Barahona, M. (2009a). Estado previo de la cuestión. In M. Arenillas, M. Barahona, M. F. Gutiérrez, & C. Cauce (Eds.), *El abastecimiento de agua a Toledo en época romana* (pp. 37–44). Confederación Hidrográfica del Tajo.

Arenillas, M., & Barahona, M. (2009b). La presa romana de La Alcantarilla en el abastecimiento de agua a Toledo. In S. Huerta, R. Soler, & A. Zaragoza (Eds.), *Actas Sexto Congr. Nac. Historia Construcción* (pp. 95–105). Inst. Juan de Herrera.

Arenillas, M., Barahona, M., & Díaz-Guerra, C. (2007). Apuntes documentales para la historia de la presa de Cornalvo. In M. Arenilas, C. Segura, F. Bueno, & S. Huerta (Eds.), *Actas Quinto Congreso Nacional Historia de la Construcción* (pp. 57–73). I. Juan de Herrera, SEdHC, CICCP, CEHOPU.

Arenillas, M., & Castillo, J. C. (2003). Dams from the Roman Era in Spain. Analysis of Design Forms (with Appendix). In S. Huerta Fernández (Ed.), *Proceedings of the First International Congress on Construction History* (pp. 243–257). Editorial Universitaria.

Arenillas, M., Hereza, J. I., Díaz-Guerra, C., & Cortés, R. (2005). La presa romana de la Virgen del Pilar (Monforte de Moyuela, Teruel). *Revista de Obras Públicas*, *3456*, 55–62.

Arenillas, M., Hereza, J. I., Dillet, J., Díaz-Guerra, C., & Cortés, R. (1995). La presa romana de Almonacid de la Cuba y otros aprovechamientos antiguos en el río Aguasvivas. *Revista de Obras Públicas*, *3345*, 42–53.

Arenillas, M., Hereza, J. I., Pintor, M. C., Cortés, R., Díaz Guerra, C., Castillo, J. C., & Pocino, S. (2006). Caracterización estructural de la presa romana de Muel. Primeros resultados. In F. Bueno, & D. Saldaña (Eds.), *Actas del II Congreso Nacional de Historia de las presas* (pp. 223–230). Editorial Universitaria.

Arenillas, M., Martín, J., & Alcaraz, A. (1992). Nuevos datos sobre la presa de Proserpina. *Revista de Obras Públicas*, *3311*, 65–69.

Baba, A. (2018). Developments in water dams and water harvesting systems throughout history in different civilizations. *International Journal of Hydrology*, *2*(2), 150166. https://doi.org/10.15406/ijh.2018.02.00064

Barahona, M. (2018a). Hacia una arqueología de las presas. Bases metodológicas para la revisión del catálogo de embalses romanos y altomedievales de la cuenca media del Tajo. In C. Pacheco (Ed.),

Actas del Congreso El Agua en la provincia de Toledo (pp. 72–86). Colectivo de Investigación Histórica Arrabal.

Barahona, M. (2018b). La red romana de captación y conducción de agua a la ciudad de Toledo: balance tras una década de investigación. In R. Rubio, J. Passini, & R. Izquierdo (Coords.), *El agua en Toledo y su entorno. Épocas romana y medieval* (pp. 30–50). Universidad de Castilla—La Mancha, Cuenca.

Barahona, M. L. (2017). *Estructuras de embalses (presas) y derivación (azudes) de épocas romana y altomedieval de la cuenca media del río Tajo* [PhD dissertation, Universidad Nacional de Educación a Distancia].

Barahona Oviedo, M., Arenillas Parra, M., & Rojas rodríguez-Malo, J. M. (2014). En torno a la red romana de abastecimiento de agua a Toledo: excavaciones en los terrenos de la Academia Militar de Infantería. *Zephyrvs*, *74*, 203–223.

Beltrán, M., & Viladés, J. M. (1994). Aquae Romanae. Arqueología de la presa de Almonacid de la Cuba. *Boletín del Museo de Zaragoza*, *13*, 127–193.

Blott, S. J., & Pye, K. (2001). GRADISTAT: A grain size distribution and statistics package for the analysis of unconsolidated sediments. *Earth Surface Processes and Landforms*, *26*(11), 1237–1248.

Burillo, F. (1980). *El valle medio del Ebro en época ibérica: contribución a su estudio en los ríos Huerva y Jiloca Medio, Zaragoza, Institución Fernando el Católico*. Zaragoza.

Burillo, F. (2005). Los Castellares de Herrera de los Navarros. In A. Chaín, & J. I. de la Torre (Eds.), *Celtíberos: tras la estela de Numancia* (pp. 109–118). Diputación Provincial de Soria.

Castillo, J. C. (2015). *Las presas romanas en España* (p. 2714). Oxford: BAR International Series.

Castillo, J. C., & Arenillas, M. (2002). Las presas romana en España. Propuesta de inventario. In S. Huerta (Ed.), *I Congreso Nacional de Historia de las presas* (pp. 199–226). Instituto Juan de Herrera.

Celestino, R. (1976). El pantano romano de Alcantarilla, en Mazarambroz. *Toletum*, *7*, 161–178.

Constante, A., Peña-Monné, J. L., & Muñoz, A. (2010). Alluvial geoarchaeology of an ephemeral stream: Implications for Holocene landscape change in the Central part of the Ebro Depression, Northeast Spain. *Geoarchaeology*, *25*(4), 475–496. https://doi.org/10.1002/gea.2031

Cuntz, O. (Ed.). (1929). Itineraria Romana, *Itineraria Romana, vol. 1: Itineraria Antonini Augusti etBurdigalense* (Vol. 1). Leipzig.

Currás, A., Zamora, L., Reed, J. M., García-Soto, E., Ferrero, S., Armengol, X., Mezquita-Joanes, F., Marqués, M. A., Riera, S., & Julià, R. (2012). Climate change and human impact in central Spain during roman times: High-resolution multi-proxy analysis of a tufa lake record (Somolinos, 1280 m asl). *Catena*, *89*, 31–53. https://doi.org/10.1016/j.catena.2011.09.009

Decker, M. J., Du Vernay, J. P., & Mcleod, J. B. (2017). Putting Roman dams in context: A virtual approach. *The International Archives of the Photogrammetry, Remote Sensing and Spatial Information Sciences*, *XLII-2/W5*, 147–153.

Dermody, B., De Boer, H. J., Bierkens, M. F. P., Weber, S. L., Wassen, M. J., & Dekker, S. C. (2011). Revisiting the humid Roman hypothesis: Novel analyses depict oscillating patterns. *Climate of the Past Discussions*, *7*(4), 2355–2389.

Dermody, B. J., van Beek, R. P. H., Meeks, E., Klein Goldewijk, K., Scheidel, W., van der Velde, Y., Bierkens, M. F. P., Wassen, M. J., & Dekker, S. C. (2014). A virtual water network of the Roman world. *Hydrology and Earth System Sciences*, *18*, 5025–5040. https://doi.org/10.5194/hess-18-5025-2014

Drdácký, M., Fratini, F., Frankeová, D., & Slížková, Z. (2013). The Roman mortars used in the construction of the Ponte di Augusto (Narni, Italy)—A comprehensive assessment. *Construction and Building Materials*, *38*(2013), 1117–1128.

Dümenil-Gates, L. (2001). Impacts of deforestation and afforestation in the Mediterranean region as simulated by the MPI atmospheric GCM. *Global and Planetary Change*, *30*, 309–328.

Dusar, B., Verstraeten, G., Notebaert, B., & Bakker, J. (2011). Holocene environmental change and its impact on sediment dynamics in the Eastern Mediterranean. *Earth-Science Reviews*, *108*, 137–157. https://doi.org/10.1016/j.earscirev.2011.06.006

Ejarque, A., Julià, R., Castanyer, P., Orengo, H. A., Palet, J. M., & Riera, S. (2022). Landscape footprints of peopling and colonisation from the Late Bronze Age to Antiquity in the coastal hinterland of Emporion-Emporiae, NE Iberia. *The Holocene*, *32*(4), 280–296. https://doi.org/10.1177/09596836211066597

Erdkamp, P. (2005). *The grain market in the Roman Empire: a social, political and economic study*. Cambridge University Press.

Erdkamp, P. (2019). Climate change and the productive landscape in the Mediterranean region in the Roman period. In P. Erdkamp, J. G. Manning, & K. Verboven (Eds.), *Climate change and ancient societies in Europe and the Hear East* (pp. 411–442). Palgrave Macmillan.

FAO. (2006). *Guidelines for soil description* (4th ed.). FAO.

Feijoo, S. (2005). Las presas y los acueductos de agua potable: una asociación incompatible en la Antigüedad. In T. Nogales (Ed.), *Augusta Emérita: territorios, espacios, imágenes y gentes en Lusitania Romana* (pp. 171–205). UNAM.

Feijoo, S. (2006). Las presas y el agua potable en época romana: dudas y certezas. In I. Moreno (Coord.), *Nuevos elementos de ingeniería romana* (pp. 145–166). Editorial Universitaria.

Fernández Casado, C. (1961). Las presas romanas en España. *Revista de Obras Públicas*, *109*, 357–363.

García-Diego, J. A., Fernández Casado, C., del Campo, C., Barredo, R., Schnitter, N., Porres, J., & del Cerro, J. (1983a). Estudio conjunto sobre la presa romana de Consuegra. *Revista de Obras Públicas*, *130*(3215), 585–599.

García-Diego, J. A., Fernández Casado, C., del Campo, C., Barredo, R., Schnitter, N., Porres, J., & del Cerro, J. (1983b). Estudio conjunto sobre la presa romana de Consuegra. *Revista de Obras Públicas*, *130*(3216), 673–688.

Giles Pacheco, F. (2011). Captación y traídas de aguas en la ciudad hispano—romana de Consabura (Consuegra, Toledo). In L. Lagóstena, J. L. Cañizar, & L Pons (Eds.), *Aquam perducendam curavit. Captación, uso y administración del agua en las ciudades de la Bética y el Occidente romano* (pp. 297–312). Editorial Universitaria.

Hajdas, I., Lindroos, A., Heinemeier, J., Ringbom, Å., Marzaioli, F., Terrasi, F., Passariello, I., Capano, M., Artioli, G., Addis, A., Secco, M., Michalska, D., Czernik, J., Goslar, T., Hayen, R., Van Strydonck, M., Fontaine, L., Boudin, M., Maspero, F., … Guibert, P. (2017). Preparation and dating of mortar samples—mortar dating inter-comparison study (MODIS). *Radiocarbon*, *59*(6), 1845–1858. https://doi.org/10.1017/RDC.2017.112

Hajdas, I., Trumm, J., Bonani, G., Biechele, C., Maurer, M., & Wacker, L. (2012). Roman ruins as an experiment for radiocarbon dating of mortar. *Radiocarbon*, *54*(3–4), 897–903. https://doi.org/10.1017/50033822200047548

Harper, K. (2017). *The fate of Rome. Climate, disease and the end of an empire*. Princeton University Press.

Harper, K., & McCormick, M. (2018). Reconstructing the Roman climate. In W. Scheidel (Ed.), *The science of Roman history. Biology, climate, and the future of the past* (pp. 11–52). New Jersey: Princenton University Press.

Hayen, R., van Strydonck, M., Fontaine, L., Boudin, M., Lindroos, A., Heinemeier, J., Ringbom, Å., Michalska, D., Hajdas, I., Hueglin, S., Marzaioli, F., Terrasi, F., Passariello, I., Capano, M., Maspero, F., Panzeri, L., Galli, A., Artioli, G., Addis, A., … Caroselli, M. (2017). Mortar dating methodology: Assessing recurrent issues and needs for further research. *Radiocarbon*, *59*(6), 1859–1871. https://doi.org/10.1017/RDC.2017.129

Hereza, I., Arenillas, M., & Cortés, R. (2000). Las presas de la cuenca del Aguasvivas. Dos mil años de regulación fluvial. In L. G. Lagóstena Barrios, J. L. Cañizar Palacios, & L. Pons Pujol (Eds.), *I Congr. Nac. Historia de las presas* (pp. 55–67). Diputación Provincial de Badajoz.

Hereza, J. I., Arenillas, M., DiazGuerra, C., & Cortés, R. (1996). *Un ejemplo histórico: el aterramiento del embalse romano de Almonacid de la Cuba*. Comité Nacional Español de Grandes Presas.

Hereza, I. (Coord.). (1996). *La presa de Almonacid de la Cuba. Del mundo romano a la Ilustración en la Cuenca del Aguasvivas*. Editorial Doce Calles.

Jansen, R. B. (1983). *Dams and Public Safety. A water resources Technical Publication*. US Department of the Interior.

Lionello, P., Malanotte-Rizzoli, P., Boscolo, R., Alpert, P., Artale, V., Li, L., Luterbacher, J., May, W., Trigo, R., Tsimplis, M., Ulbrich, U., & Xoplaki, E. (2006). The Mediterranean climate: An overview of the main characteristics and issues. In P. Lionello, P. Malanotte-Rizzoli, & R. Boscolo (Eds.), *Mediterranean Climate variability* (pp. 1–26). Elsevier.

Ljungqvist, F. C. (2010). A new reconstruction of temperature variability in the extra-tropical Northern Hemisphere during the last two millennia. *Geografiska Annaler: Series A, Physical Geography*, *92*(3), 339–351.

Lubritto, C., Ricci, P., Germinario, C., Izzo, F., Mercurio, M., Langella, A., Cuenca, V. S., Torres, I. M., Fedi, M., & Grifa, C. (2018). Radiocarbon dating of mortars: Contamination effects and sample characterisation. The case-study of Andalusian medieval castles (Jaén, Spain). *Measurement*, *118*, 362–371. https://doi.org/10.1016/j.measurement.2017.10.046

Luterbacher, J., García-Herrera, R., Akcer-On, S., Allan, R., Alvarez-Castro, M. C., Benito, G., Booth, J., Büntgen, U., Cagatay, N., Colombaroli, D., Davis, B., Esper, J., Felis, T., Fleitmann, D., Frank, D., Gallego, D., Garcia-Bustamante, E., Glaser, R., Gonzalez-Rouco, F. J., & Zorita, E. (2012). A Review of 2000 Years of Paleoclimatic Evidence in the Mediterranean. In P. Lionello (Ed.), *The climate of the Mediterranean region. From the past to the future* (pp. 88–186). Elsevier.

Magallón, M. A. (1987). *La red viaria romana en Aragón*. Diputación General de Aragón.

Magallón, M. A., Uribe, P., & Fanlo, J. (2016). La presa romana de Muel (Zaragoza). In J. I. Lorenzo, & J. M. Rodanés (Eds.), *Actas del I Congreso de Arqueología y Patrimonio Aragonés* (pp. 399–409). Universidad de Zaragoza.

Martín Morales, J., Arenillas, M., Cortés, R., Díaz-Guerra, C., & Arenillas Girola, L. (2002). La presa de Cornalbo en Mérida. In F. Bueno (Ed.), *Actas del I Congreso de Historia de las presas* (pp. 279–287). Diputación Provincial de Badajoz.

Martín-Puertas, C., Valero-Garcés, B. L., Achim Brauer, A., Mata, M. P., Delgado-Huertas, A., & Dulski, P. (2008). The Iberian–Roman Humid Period (2600–1600 cal yr BP) in the Zoñar Lake varve record (Andalucía, Southern Spain). *Quaternary Research*, *71*(21), 108–120. https://doi.org/10.1016/j.yqres.2008.10.004

Mays, L. W. (2008). A very brief history of hydraulic technology during antiquity. *Environmental Fluid Mechanics*, *8*, 471–484. https://doi.org/10.1007/s10652-008-9095-2

Mays, L. W. (2010). A brief history of Roman water technologies. In L. W. Mays (Ed.), *Ancient water technologies* (pp. 115–137). Springer.

McCormick, M., Büntgen, U., Cane, M. A., Cook, E. R., Harper, K., Huybers, P., Litt, T., Manning, S. W., Mayewski, P. A., More, A. F. M., Nicolussi, K., & Tegel, W. (2012). Climate change during and after the roman empire: Reconstructing the past from scientific and historical evidence. *The Journal of Interdisciplinary History*, *43*(2), 169–220. https://doi.org/10.1162/JINH_a_00379

Miriello, D., Barca, D., Bloise, A., Ciarallo, A., Crisci, G. M., De Rose, T., Gattuso, C., Gazineo, F., & La Russa, M. F. (2010). Characterisation of archaeological mortars from Pompeii (Campania, Italy) and identification of construction phases by compositional data analysis. *Journal of Archaeological Science*, *37*(9), 2207–2223.

Nelson, R. E., & Sommers, L. E. (1982). Total carbon and organic matter. In A. L. Page, R. H. Miller, & D. R. Keeney (Eds.), *Methods of soil analysis. Part 2: Chemical and microbiological properties*, 2nd edition (pp. 539–557). American Society of Agronomy.

Notebaert, B., Berger, J. F., & Brochier, J. L. (2014). Characterization and quantification of Holocene colluvial and alluvial sediments in the Valdaine Region (southern France. *The Holocene*, *24*, 1320–1335. https://doi.org/10.1177/0959683614540946

Peña Monné, J. L. (1997). *Cartografía geomorfológica básica y aplicada*. Ed. Geoforma.

Peña Monné, J. L. (2018). Geoarqueología aplicada a la reconstrucción paleoambiental: La evolución del Holoceno superior en el NE de España. *Boletín Geológico y Minero*, *1129*(1/2), 285–303. https://doi.org/10.21701/bolgeomin.129.1.011

Peña Monné, J. L., Cuadrat, J. M., & Sánchez Fabre, M. (2002). *El clima de la provincia de Teruel*. Instituto de Estudios Turolenses.

Peña Monné, J. L., Gutiérrez, M., Ibáñez, M. J., Lozano, M. V., Rodriguez, J., Sánchez, M., Simón, J. L., Soriano, M. A., & Yetano, L. M. (1984). *Geomorfología de la provincia de Teruel*. Instituto de Estudios Turolenses.

Peña-Monné, J. L., Julián, A., Chueca, J., Echeverría, M. T., & Ángeles, G. (2004). Etapas de evolución holocena en el valle del río Huerva: Geomorfología y Geoarqueología. In J. L. Peña-Monné, L. A. Longares, & M. Sánchez Fabre (Eds.), *Geografía Física de Aragón. Aspectos generales y temáticos* (pp. 289–302). Univ. Zaragoza e Inst. Fernando el Católico.

Peña-Monné, J. L., & Sampietro-Vattuone, M. M. (2019). Late Holocene anthropic degradation records in semi-arid environments (NE Spain and NW Argentina). *Cuadernos de Investigación Geográfica*, *45*(1), 195–217. https://doi.org/10.18172/cig.3587

Pueyo, E., Mauritsch, H., Pocoví, A., Scholger, R., Millán, H., & Valero, B. (2001). Archaeomagnetostratigraphy of the filling of a Roman dam. In C. M. Batt, I. Zanari, & D. H. Tarling (Eds.), *Archaeomagnetism applied to the rescue of cultural heritages* (p. 328). University of Loeben.

Pueyo, E. L., Silva Aguilera, C., Beamud, B., & Valero-Garcés, B. (2008). Archaeomagnetostratigraphy; a dating tool in ancient dams sediments. A case study in the Muel Roman reservoir (Northern Spain). *Geo-Temas*, *10*, 1187–1190.

Quintela, A. C., Cardoso, J. L., & Mascarenhas, J. M. (1987).Roman dams in Southern Portugal. *International Water Power and Dam Construction*, *1*, 38–40.

Reale, O. (2000). Modeling the effects of vegetation on Mediterranean climate during the Roman Classical Period: Part II: Model simulation. *Global and Planetary Change*, *25*, 185–214.

Reale, O. (2000). Modeling the effects of vegetation on Mediterranean climate during the Roman Classical Period—Part I: Climate history and model sensitivity. *Global and Planetary Change*, *25*, 163–184.

Reimer, P. J., Austin, W. E. N., Bard, E., Bayliss, A., Blackwell, P. G., Bronk Ramsey, C., Butzin, M., Cheng, H., Edwards, R. L., Friedrich, M., Grootes, P. M., Guilderson, T. P., Hajdas, I., Heaton, T. J., Hogg, A. G., Hughen, K. A., Kromer, B., Manning, S. W., Muscheler, R., … Talamo, S. (2020). The IntCal20 Northern Hemisphere radiocarbon age calibration curve (0–55 cal kBP. *Radiocarbon*, *62*(4), 725–757. https://doi.org/10.1017/RDC.2020.41

Rietveld, H. M. (1969). A profile refinement method for nuclear and magnetic structures. *Journal of Applied Crystallography*, *2*, 65–71.

Ringbom, Å., Lindroos, A., Heinemeier, J., & Sonck-Koota, P. (2014). 19 years of mortar dating: Learning from experience. *Radiocarbon*, *56*(2), 619–635. https://doi.org/10.2458/56.17469

Rodríguez Simón, P., & Díez de Pinos López, E. (2015). La ciudad romana de El Pueyo de Belchite: nuevas investigaciones. *Salduie*, *15*, 213–232.

Rodríguez Untoria, S. (2011). Estudio arqueológico de la presa romana de Consuegra (Toledo). In L. G. Lagóstena Barrios, J. L. Cañizar Palacios,

& L. Pons Pujol (Eds.), *Actas Congreso Int. Aquam perdvcendam cvravit. Captación, uso y administración del agua en las ciudades de la Bética y el Occidente romano* (pp. 313–332). Universidad de Cádiz.

Rodríguez-Carvajal, J. (1993). Recent advances in magnetic structure determination by neutron powder diffraction. *Physica B: Condensed Matter*, *192*, 55–69.

Royo, J. I. (2010). La Malena: una villa tardorromana excepcional. In J. Cinca, & J. L. Ona (Coord.), *Comarca de Campo de Belchite* (pp. 173–182). Gobierno de Aragón.

Royo Guillén, J. I. (1992). La villa tardorromana de "La Malena" en Azuara y el mosaico de las Bodas de Cadmo y Harmonia. *Journal of Roman Archaeology*, *5*, 148–161.

Ruiz Fernández de la Lopa, V., & Carls, P. (1985). *Mapa Geológico de España serie MAGNA 1:50000, hoja 466 (Moyuela)*. Instituto Geológico Minero de España.

Saldaña, D. (2011). *Presas de mampostería en España. Tesis doctoral. Escuela de Ingenieros de Caminos, Canales y Puertos* [PhD dissertation, Universidad de Cantabria].

Sánchez, E., & Martínez, J. (2016). *Los acueductos de Hispania: construcción y abandono*. Fundación Juanelo Turriano.

Sánchez Abal, J. L. (1977). Obra hidráulica romana en la provincia de Toledo (Pantano de Alcantarilla). In Universidad de Barcelona, Instituto deArqueología y Prehistoria, Caja Segovia (Eds.), *Segovia y la arqueología romana* (pp. 359–366). Editorial Universitaria.

Schnetz, J., (Ed.). (1940). *Itineraria Romana. Volumen alterum, Ravennatis anonymi cosmographia et Guidonis geographica*.

Schnitter, N. J. (1994). *A history of dams, the useful pyramids*. Balkema Publishers.

Silva Aguilera, C., Hinderer, M., Valero-Garcés, B., Pueyo, E., & Hornung, J. (2008). The siltation history of the Muel Roman dam (NE Spain). *Geo-Temas*, *10*, 191–193.

Simón, J. M. (1992). Prospecciones arqueológicas en la Sierra y Campo de Loscos.Campaña de 1990. *Arqueología Aragonesa*, *1990*, 307–331.

Smith, A. F. (1970). *The Heritage of Spanish Dams. Servicio de Publicaciones del Colegio de Ingenieros de Caminos, Canales y Puertos*. Colegio de Ingenieros de Caminos.

Smith, N. (1971). *A history of dams*. Davies.

Urbanová, P., & Guibert, P. (2017). Methodological study on single grain OSL dating of mortars: Comparison of five reference archaeological sites. *Geochronometria*, *44*(1), 77–97. https://doi.org/10.1515/geochr-2015-0050

Urbanova, P., Hourcade, D., Ney, C., & Guibert, P. (2015). Sources of uncertainties in OSL dating of archaeological mortars: The case study of the Roman amphitheatre Palais-Gallien in Bordeaux. *Radiation Measurements*, *72*, 100–110. https://doi.org/10.1016/j.radmeas.2014.11.014

Uribe, P., Fanlo, J., Magallón, M. A., & Angás, J. (2013). Le barrage de Muel (Saragosse, Espagne). In F. Baratte, J. L. Robin, & L. Rocca (Eds.), *Regards croisés d'Orient et d'Occident. Les barrages dans l'Antiquité Tardive. Collection Orient & Méditerranée* (pp. 197–228). Sorbonne.

Uribe, P., Magallón, A., & Fanlo, J. (2012). New evidence on Roman water supply in the Ebro Valley: The Roman Dam of Muel (Zaragoza, Spain). In M. Zuchowska (Ed.), *The archaeology of water supply* (pp. 75–83). BAR.

Uribe, P., Magallón, M. A., Fanlo, J., Martínez Bea, M., Domingo, R., Reklaityte, I., & Pérez-Lambán, F. (2010). La presa romana de Muel: novedades de hidráulica romana en el Valle del Ebro. In L. G. Lagóstena, J. L. Cañizar, & L. Pons (Eds.), *Aqvam perdvcendam curavit. Captación, uso y administración del agua en las ciudades de la Bética y el Occidente romano* (pp. 333–346). Fac. Filosofía Universidad de Cádiz.

Uribe Agudo, P., Magallón, M. Á., Navarro Caballero, M., & Fanlo Loras, J. (2016). Nuevas marcas epigráficas procedentes de la presa romana de Muel (Zaragoza). *Salduie*, *16*, 209–245.

Utrilla, J. F. (2010). El Campo de Belchite en la Edad Media (s. VIII/XV): del poblamiento musulmán al cristiano. In J. Cinca, & J. L. Ona (Eds.), *Comarca de Campo de Belchite* (pp. 83–99). Zaragoza.

Visher, G. S. (1969). Grain size distributions and depositional processes. *Journal of Sedimentary Research*, *39*(3), 1074–1106.

Young, R. A. (1995). *The Rietveld method, International Union of Crystallography*. Oxford University Press.

How to cite this article: Peña-Monné, J. L., Sampietro-Vattuone, M. M., Paula, U. A., García Giménez, R., Muñoz, A., Villas, D. B., & Magallón Botaya, M. Á. (2023). Structure, evolutionary context and chronological data of the Monforte de Moyuela Roman dam (Ebro Basin, NE of Spain). *Geoarcheology*, 38, 482–509. https://doi.org/10.1002/gea.21953